

1     **A data-based predictive model for spatio-temporal**  
2             **variability in stream water quality**

3     Danlu Guo<sup>1</sup>, Anna Lintern<sup>1,2</sup>, J. Angus Webb<sup>1</sup>, Dongryeol Ryu<sup>1</sup>, Ulrike Bende-Michl<sup>3</sup>, Shuci Liu<sup>1</sup>,  
4                             Andrew William Western<sup>1</sup>

5     <sup>1</sup> Department of Infrastructure Engineering, The University of Melbourne, Parkville, VIC Australia;

6     <sup>2</sup> Department of Civil Engineering, Monash University, Clayton, VIC Australia

7     <sup>3</sup> Bureau of Meteorology, Parkes, ACT Australia.

8     Corresponding author's email: danlu.guo@unimelb.edu.au

9

## 10 **Abstract**

11 Our current capacity to model stream water quality is limited particularly at large spatial scales across  
12 multiple catchments. To address this, we developed a Bayesian hierarchical statistical model to simulate  
13 the spatio-temporal variability in stream water quality across the state of Victoria, Australia. The model  
14 was developed using monthly water quality monitoring data over 21 years, across 102 catchments, which  
15 span over 130,000 km<sup>2</sup>. The modelling focused on six key water quality constituents: total suspended  
16 solids (TSS), total phosphorus (TP), filterable reactive phosphorus (FRP), total Kjeldahl nitrogen  
17 (TKN), nitrate-nitrite (NO<sub>x</sub>), and electrical conductivity (EC). The model structure was informed by  
18 knowledge of the key factors driving water quality variation, which had been identified in two preceding  
19 studies using the same dataset. Apart from FRP, which is hardly explainable (19.9%), the model explains  
20 38.2% (NO<sub>x</sub>) to 88.6% (EC) of total spatio-temporal variability in water quality. Across constituents,  
21 the model generally captures over half of the observed spatial variability; temporal variability remains  
22 largely unexplained across all catchments, while long-term trends are well captured. The model is best  
23 used to predict proportional changes in water quality in a Box-Cox transformed scale, but can have  
24 substantial bias if used to predict absolute values for high concentrations. This model can assist  
25 catchment management by (1) identifying hot-spots and hot moments for waterway pollution; (2)  
26 predicting effects of catchment changes on water quality e.g. urbanization or forestation; and (3)  
27 identifying and explaining major water quality trends and changes. Further model improvements should  
28 focus on: (1) alternative statistical model structures to improve fitting for truncated data, for constituents  
29 where a large amount of data below the detection-limit; and (2) better representation of non-conservative  
30 constituents (e.g. FRP) by accounting for important biogeochemical processes.

## 31 **Keywords**

32 stream water quality; spatio-temporal variability; sediments; nutrients; statistical modeling; Bayesian  
33 hierarchical model

34

## 35        **1. Introduction**

36        Deteriorating water quality in aquatic systems such as rivers and streams can have significant  
37        environmental, economic and social ramifications (e.g. Whitworth et al., 2012;Vörösmarty et al.,  
38        2010;Qin et al., 2010;Kingsford et al., 2011). Reducing these impacts requires effective management  
39        and mitigation of poor water quality; however, high variability in water quality both across space and  
40        time reduces our ability to accurately assess the status of water quality and to develop effective  
41        management strategies. Thus, improved modelling frameworks to predict and interpret this variability  
42        would be useful for water quality management (Chang, 2008;Ai et al., 2015;Zhou et al., 2012).

43        Water quality conditions can vary across individual events, as well as at daily, seasonal and inter-annual  
44        scales at an individual location (Arheimer and Lidén, 2000; Kirchner et al., 2004; Larned et al., 2004;  
45        Pellerin et al., 2012; Saraceno et al., 2009). Water quality conditions also typically differ substantially  
46        across locations (Meybeck and Helmer, 1989;Chang, 2008;Varanka et al., 2015;Lintern et al., 2018a).  
47        These variabilities in stream water quality are driven by three key mechanisms: (1) source, which defines  
48        the total amount of constituents being available in a catchment; (2) mobilization, which detaches  
49        constituents (both in particulate and dissolved forms) from their sources via processes such as erosion  
50        and biogeochemical processing; and (3) delivery of mobilized constituents from catchments to receiving  
51        waters via multiple hydrologic pathways including surface and subsurface flow (Granger et al., 2010).

52        Spatial variability in stream water quality is driven by human activities within catchments (e.g., land use  
53        and management, vegetation cover etc.) (Lintern et al., 2018a;Carey and Migliaccio, 2009;Giri and Qiu,  
54        2016;Heathwaite, 2010), along with natural catchment characteristics such as climate, geology, soil  
55        type, topography and hydrology (Hrachowitz et al., 2016;Poulsen et al., 2006;Sueker et al.,  
56        2001;Onderka et al., 2012). At the same time, temporal shifts in water quality are also influenced by  
57        changes in pollutant sources, such as land use and land management including urbanization, agriculture  
58        and vegetation clearing (Ren et al., 2003;Smith et al., 2013;Ouyang et al., 2010). In addition, water  
59        quality can also vary in time with variations in the mobilization and delivery processes, which are largely  
60        driven by the hydro-climatic conditions at a catchment, such as streamflow (Ahearn et al.,  
61        2004;Mellander et al., 2015;Sharpley et al., 2002;Zhang and Ball, 2017), the timing and magnitude of  
62        rainfall events (Fraser et al., 1999;Miller et al., 2014) and temperature (Bailey and Ahmadi, 2014).

63 As abovementioned, we have good understanding of the key controls for variations in water quality,  
64 albeit in an isolated, idealized context. We still lack a sound understanding of how relationships between  
65 specific landscape characteristics and water quality can shift with influences from other landscape  
66 characteristics, and how the drivers of temporal variability in water quality can interact and vary across  
67 large spatial scales (Musolff et al., 2015;Lintern et al., 2018a;Ali et al., 2017). In contrast, current  
68 detailed understanding have been primarily based on field studies at small scales with detailed  
69 information on specific temporal drivers ranging from hydrologic conditions to detailed management  
70 decisions such as fertilizer rates and application timing (Smith et al., 2013;Poudel et al., 2013;Adams et  
71 al., 2014). While operational weather observation networks, stream gauging networks and remote  
72 sensing can provide some of this information, developing a large-scale understanding of water quality  
73 patterns across catchments would ideally also involve an extensive suite of management information  
74 that substantially exceeds what is currently available.

75 Due to the limited understanding of large-scale water quality patterns, we currently lack the capacity to  
76 model spatio-temporal variabilities in water quality at large scales across multiple catchments. This  
77 hinders our ability to inform the development of effective policy and mitigation strategies over large  
78 regions. Specifically, conceptual or physically-based water quality models are typically limited by the  
79 simplification of physical processes such as flow pathways (Hrachowitz et al., 2016). Furthermore,  
80 practical implementation of these models can be also limited by the intensive data requirements for  
81 calibration and validation, particularly for large regions with highly heterogeneous catchment conditions  
82 (Fu et al., 2018;Abbaspour et al., 2015). In contrast, when performed over large geographical regions,  
83 statistical water quality models are generally more capable of simulating water quality variability while  
84 requiring less detailed information and thus effort for implementation. However, existing statistical  
85 models often focus only on either the spatial variation of time-averaged water quality conditions  
86 (Tramblay et al., 2010;Ai et al., 2015) or the temporal variation at individual locations (Kisi and Parmar,  
87 2016;Kurunç et al., 2005;Parmar and Bhardwaj, 2015), which often limits their value as practical  
88 management tools. Modelling the spatio-temporal variability simultaneously remains challenging over  
89 long time periods and large regions.

90 Accordingly, this research attempts to bridge the gap between fully-distributed physically-based water

91 quality models and data-driven statistical approaches. We aim to develop a process-informed, data-  
92 driven model to predict spatio-temporal changes in stream water quality over a large region consisting  
93 of multiple catchments. Specifically, this model was established using long-term (21 years) stream water  
94 quality observations across 102 catchments in Australia, with an aggregate catchment area of 130,000  
95 km<sup>2</sup>. To obtain the necessary understanding of process drivers required to develop this model, two  
96 preceding studies were conducted on the same dataset to identify the key drivers for the spatial and  
97 temporal variability of water quality, respectively (Lintern et al., 2018b; Guo et al., 2019). The aim of  
98 this study is to develop an integrated spatio-temporal model using the previously-identified spatial and  
99 temporal predictors, and to then assess the performance of this model. Spatio-temporal variability of  
100 water quality was modelled using a novel Bayesian hierarchical approach which can jointly account for  
101 both variability components, including accounting for varying temporal water quality dynamics between  
102 catchments. This modelling approach also has relatively low requirement for input data, which keeps  
103 the modelling detail commensurate with the level of data availability. During the model development,  
104 we also obtained additional understanding on the patterns of spatial variations in the effects of each  
105 temporal predictor. The model can potentially provide useful information for large-scale catchment  
106 management, assessment and policy making, such as testing major changes in land use patterns,  
107 informing pollution hot-spots, as well as identification and attribution of water quality trends and  
108 changes over time.

## 109 **2. Method**

110 We first discuss the process used to develop the integrated spatio-temporal model (Section 2.1). Sections  
111 2.1.1 and 2.1.2 introduces the statistical modelling framework and the data used for model development,  
112 respectively. The approaches to determine model structure was then introduced, which include the  
113 choice of key predictors (Section 2.1.3) and the calibration for model parameters (Section 2.1.4). Finally,  
114 the approaches to evaluate model performance and robustness are described in Section 2.2.

### 115 **2.1 Model development**

#### 116 **2.1.1 Spatio-temporal modelling framework**

117 A Bayesian hierarchical approach was used to model the spatio-temporal variability in stream water  
118 quality. The Bayesian approach enables the inherent natural stochasticity of water quality to be

119 incorporated into the model (Clark, 2005). A key strength of applying the hierarchical model structure  
 120 to analyze spatio-temporal variability is that this structure enables the key controls of temporal  
 121 variability in water quality to vary across locations (Webb and King, 2009;Borsuk et al., 2001). This  
 122 variability has been found to be important in other study regions where the (temporal) solute export  
 123 regime varies with catchment characteristics such as climate and land use (Musolff et al., 2015;Poor and  
 124 McDonnell, 2007).

125 The structure of the Bayesian hierarchical model is presented below in Eq. 1 to 6. Eq. 1 formulates the  
 126 transformed constituent concentration (see Section 2.1.2 for justification) at time  $i$  and site  $j$  ( $C_{ij}$ ) as a  
 127 normally distribution with a mean  $\mu_{ij}$  and standard deviation  $\sigma$  representing inherent randomness.

$$C_{ij} \sim N(\mu_{ij}, \sigma) \quad (1)$$

128 To represent spatio-temporal variability,  $\mu_{ij}$  is modelled as the sum of the site-level mean constituent  
 129 concentration ( $\bar{C}_j$ ) and the deviation from that mean at time  $i$  ( $\Delta_{ij}$ ) (Eq. 2).

$$\mu_{ij} = \bar{C}_j + \Delta_{ij} \quad (2)$$

130 To describe spatial variability, the site-level mean concentration at site  $j$  ( $\bar{C}_j$ ) is modelled as a linear  
 131 function of a global intercept ( $intC$ ), and the sum of  $m$  catchment characteristics  $S_{1,j}$  to  $S_{m,j}$  (e.g. land  
 132 use, topography) weighted by their relative contributions to spatial variability ( $\beta S_1$  to  $\beta S_m$ ) (Eq. 3).

$$\bar{C}_j = intC + \beta S_1 \times S_{1,j} + \beta S_2 \times S_{2,j} + \dots + \beta S_m \times S_{m,j} \quad (3)$$

133 The temporal variability, represented by the deviation from the mean ( $\Delta_{ij}$ ), is a linear combination of  $n$   
 134 temporal variables,  $T_{1,ij}$  to  $T_{n,ij}$  (e.g., climate condition, streamflow, vegetation cover) (Eq. 4), at time  
 135  $i$  and site  $j$ .

$$\Delta_{ij} = \beta T_{1,j} \times T_{1,ij} + \dots + \beta T_{n,j} \times T_{n,ij} \quad (4)$$

136 The selection of key spatial and temporal predictors for the model has been performed in our two  
 137 preceding studies (Lintern et al., 2018b; Guo et al., 2019) and is briefly described in Section 2.1.3. Eq.  
 138 1 to 4 enable the model to separately represent the spatial and temporal variability in water quality;  
 139 however, there is still a further step required to make the model fully spatio-temporal (i.e. being able to  
 140 predict over both time and location). Specifically, in Guo et al. (2019), clear spatial variation was  
 141 observed in the relationships between water quality and its key temporal predictors (i.e. in the  $\beta T_{N,j}$  in

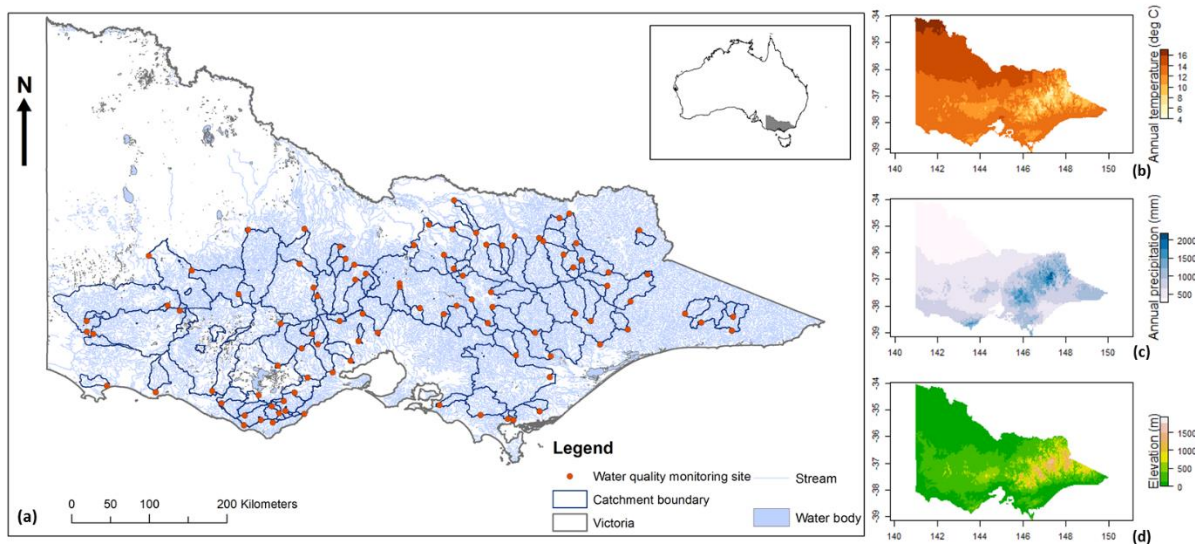
142 Eq. 4). To be able to model multiple catchments across a large spatial area simultaneously, we must  
 143 account for differences in these temporal influences across sites. To do this, the effect of each temporal  
 144 variable at site  $j$  ( $\beta T_{N,j}$  with  $N$  in  $1, 2, \dots, n$ ) is drawn from a distribution with a mean of  $\mu\beta T_{N,j}$  (Eq. 5),  
 145 which is then modelled with a linear combination of two additional catchment characteristics,  $ST_{N1,j}$   
 146 and  $ST_{N2,j}$  (Eq. 6). Details of the selection for these two additional predictors are presented in Section  
 147 2.1.3.

$$\beta T_{N,j} \sim N(\mu\beta T_{N,j}, \sigma\beta T), \text{ for } N \text{ in } 1, 2, \dots, n \quad (5)$$

$$\mu\beta T_{N,j} = \text{int}\beta T_N + \beta ST_{N1} \times ST_{N1,j} + \beta ST_{N2} \times ST_{N2,j} \quad (6)$$

#### 148 2.1.2 Data collection and processing

149 The Bayesian hierarchical model was developed with 21 years of monthly stream water quality  
 150 observations at 102 catchments in the state of Victoria, Australia (aggregate catchment area  $> 130,000$   
 151  $\text{km}^2$ ). The collection and processing of the data are detailed in previous publications that worked with  
 152 the same dataset (Lintern et al., 2018b; Guo et al., 2019). Briefly, stream water quality data were  
 153 extracted from the Victorian Water Measurement Information System (Department of Environment  
 154 Land Water and Planning (DELWP) Victoria, 2016b), which contains monthly grab samples of water  
 155 quality at approximately 400 sites across Victoria. Water quality data sampled between 1994 and 2014  
 156 at 102 sites were used to develop the model (Fig. 1). These sites and time period were chosen because  
 157 they provided the longest consistent period of continuous records over the greatest number of monitoring  
 158 sites. The catchments corresponding to these water quality monitoring sites were delineated using the  
 159 Geofabric tool (Bureau of Meteorology, 2012), and have areas ranging from  $5 \text{ km}^2$  to  $16,000 \text{ km}^2$ . The  
 160 water quality parameters of interest were: total suspended solids (TSS), total phosphorus (TP), filterable  
 161 reactive phosphorus (FRP), total Kjeldahl nitrogen (TKN), nitrate-nitrite ( $\text{NO}_x$ ) and electrical  
 162 conductivity (EC). These parameters represent sediments, nutrients and salts, which are some of the key  
 163 concerns for water quality managers in Australia and around the world. These water quality samples  
 164 were collected following standard DELWP protocols (Australian Water Technologies, 1999) and  
 165 analysed in National Association of Testing Authorities accredited laboratories. Note that in the  
 166 sampling protocol, FRP is defined as ‘*Reactive Phosphorus for a filtered sample to a defined filter size*  
 167 (*e.g. RP( $<0.45 \mu\text{m}$ )*)’, which is equivalent to the more widely-used terminology, SRP i.e. Soluble  
 168 Reactive Phosphorus (Jarvie et al., 2002).



169

170 **Figure 1. Map of (a) the 102 selected water quality monitoring sites and their catchment**  
 171 **boundaries, with inserts showing the location of the state of Victoria within Australia; (b) annual**  
 172 **average temperature and (c) annual precipitation and (d) elevation across Victoria.**

173 To compile a dataset for the potential spatial explanatory variables (i.e. predictors to explain spatial  
 174 variability in water quality), a comprehensive literature review was conducted (Lintern et al., 2018a),  
 175 which summarized the key catchment landscape characteristics that are widely known to influence  
 176 water quality. Further, as part of Lintern et al. (2018b), fifty potential explanatory catchment  
 177 characteristics were selected, which included catchment land use, land cover, topographic, climatic,  
 178 geological, lithological and hydrological catchment characteristics. These variables were derived using  
 179 datasets obtained from Geoscience Australia (2004, 2011), the Bureau of Meteorology (2012), the  
 180 Bureau of Rural Sciences (2010), Department of Environment Land Water and Planning Victoria (2016)  
 181 and the Terrestrial Ecosystem Research Network (2016) (see Table S1 in the Supplementary Material  
 182 for detailed variable names and data sources). We used a static set of land use data from 2005-2006 to  
 183 represent the entire study period, as a preliminary analysis between 1996 and 2011 suggested less than  
 184 1% changes in the key land uses in these catchments (i.e. agricultural, grazing, conservation).

185 Nineteen potential temporal explanatory variables were included. Firstly, data of discharge (originally  
 186 in  $\text{ML d}^{-1}$ ) and water temperature ( $^{\circ}\text{C}$ ) corresponding to the same timestamps for water quality  
 187 observations were also extracted for each monitoring site over the study period (Department of  
 188 Environment Land Water and Planning Victoria, 2016). Discharge was converted to runoff depth ( $\text{mm}$   
 189  $\text{d}^{-1}$ ) for each catchment, and the average streamflows over 1, 3, 7, 14 and 30 days preceding the water  
 190 quality sampling dates were calculated. In addition, we extracted gridded dataset from the Australian



191 Water Availability Project (AWAP) (Frost et al., 2016;Raupach et al., 2009, 2012) and Australian Water  
192 Resources Assessment Landscape (AWRA-L) model (Frost et al., 2016). These datasets were used to  
193 calculate catchment averaged values of daily average temperature ( $^{\circ}\text{C}$ ), daily rainfall (mm), antecedent  
194 rainfall (1, 3, 7, 14 and 30 days preceding sampling), dry spell ( $> 0.1\text{mm}$  rainfall) length in the antecedent  
195 14 days, daily actual evapotranspiration (ET) (mm), as well as soil moisture for the root-zone and the  
196 deep-zone (averaged volumetric content for shallower and deeper than 1m, respectively). In addition,  
197 catchment averaged monthly NDVI data were extracted from Advanced Very High Resolution  
198 Radiometer (AVHRR) Product (Eidenshink, 1992) and Moderate Resolution Imaging  
199 Spectroradiometer MOD13A3 (NASA LP DAAC, 2017). A summary of these datasets of temporal  
200 variables and their corresponding sources are in Table S2 in the Supplementary Material and details are  
201 provided in Guo et al. 2019.

202 The raw input data were filtered and transformed to increase the data reliability, continuity and  
203 symmetry, making them more suitable for use in the linear spatio-temporal model structure (Eq. 3, 4  
204 and 6). For the filtering process, we first removed all water quality records with flags indicating quality  
205 issues. We also removed any values below the detection limit (DL), which was defined as the '*minimum  
206 concentration detected for which there is 95% confidence of accuracy and therefore is accurate enough  
207 to report*' in the monitoring protocols for this dataset (Australian Water Technologies, 1999). This was  
208 because the uncertainty in values below the DL would be amplified after transformation, which would  
209 influence the subsequent model fitting. Furthermore, those undetectable low concentrations were of less  
210 interest for management purposes. Water quality records corresponding to days with zero flows were  
211 also excluded from further analyses.

212 The transformation process was performed for each of the spatial catchment characteristics, temporal  
213 explanatory variables, as well as each water quality constituent to improve the symmetry of individual  
214 distributions. The log-sinh transformation (Wang et al., 2012) (Eq. 7) was used for all catchment  
215 characteristics, due to its ability to resolve the presence of zero values in several of the catchment  
216 characteristics (e.g., percentage area of individual land uses). The *GA* package in R (Luca Scrucca, 2019)  
217 was used to identify the log-sinh transformation parameters ( $a$  and  $b$ ) for each spatial explanatory  
218 variable that minimized the data skewness (i.e. symmetry is maximized) across all 102 catchments.

219 
$$y_{log-sinh} = \frac{1}{b} \log(\sinh[a + by_{raw}]) \quad (7)$$

220 In addition, all observed constituent concentrations and temporal explanatory variables were Box-Cox  
 221 transformed (Box and Cox, 1964) (Eq. 8).

222 
$$y_{Box-Cox} = \begin{cases} \frac{y_{Raw}^\lambda - 1}{\lambda}, & \text{for } \lambda \neq 0 \\ \log y, & \text{for } \lambda = 0 \end{cases} \quad (8)$$

223 For each variable, the optimal Box-Cox transformation parameter  $\lambda$  was identified using the *car* R  
 224 package and a maximum likelihood-like approach. We first identified the optimal Box-Cox parameter  $\lambda$   
 225 using the data at each site (i.e. 21-year time-series). The averaged  $\lambda$  across all sites was then used to  
 226 transform the data across all catchments together. This transformation approach ensured that all sites  
 227 used a consistent transformation parameter. All transformation parameters used are summarized in  
 228 Tables S3 and S4 in the Supplementary Material. The transformation process has greatly improved the  
 229 data symmetry and thus suitability for use in a linear model (the quality of the transformations was  
 230 assessed via visual inspection in Lintern et al., 2018b; Guo et al., 2019; and summarized in Figures S2,  
 231 S4 and S6 in the Supplementary Material).

### 232 2.1.3 Selection of key model predictors

233 Key predictors for the model were selected in a process-informed and data-driven manner based on our  
 234 two preceding studies (Lintern et al., 2018b; Guo et al., 2019). Lintern et al. (2018b) identified the best  
 235 spatial predictors ( $S_1$  to  $S_m$  in Eq. 3) for the model, while the best temporal predictors across all sites  
 236 ( $T_1$  to  $T_n$  in Eq. 4) have been identified in Guo et al., (2019). In both studies, the best predictors were  
 237 selected using an exhaustive search approach (May et al., 2011; Saft et al., 2016), which considered all  
 238 possible combinations of the potential predictors introduced earlier in this section. This selection  
 239 approach required firstly fitting an individual model to all possible candidate predictor sets, and then  
 240 comparing all fitted models to select a single best set of predictors. Alternative models were evaluated  
 241 based on the Akaike Information Criterion (AIC) (Akaike, 1974) and Bayesian Information Criterion  
 242 (BIC) (Schwarz, 1978) to ensure optimal balance between model performance and complexity.

243 The best predictors to explain the spatial and temporal variabilities in each constituent are listed in Table  
 244 1. Generally speaking, the key factors controlling the spatial variability in river water quality were land-  
 245 use and long-term climate conditions (Lintern et al., 2018b). Temporal variability was mainly explained

246 by temporal changes in streamflow conditions, water temperature and soil moisture (Guo et al., 2019).  
247 The potential mechanisms via which these key drivers influence water quality are discussed in details  
248 in these two previous studies.

249 **Table 1. Key factors affecting the spatial and temporal variability for each of six constituents, as identified**  
250 **in Lintern et al. (2018) and Guo et al. (2019b), respectively.**

251  
252 Whilst the previous studies (Lintern et al. 2018b, Guo et al. 2019) identified the predictors for spatial  
253 and temporal variability respectively, they did not provide guidance on the predictors for spatial  
254 variability in the relationships between drivers of temporal variability and temporal water quality  
255 response (i.e.  $\beta T$  in Eq 4). As such, the final step of the predictor selection process to develop the  
256 combined spatio-temporal model was to identify the key catchment characteristics that affect spatial  
257 variability in the hydroclimatic parameters driving temporal changes in water quality ( $\beta T_l$  to  $\beta T_n$  in Eq.  
258 4, also right column in Table 1). This is achieved by selecting two spatial characteristics that are most  
259 closely related to the coefficient for each temporal predictor ( $ST_{N1}$  and  $ST_{N2}$ , Eq. 6) across all sites,  
260 where only two spatial characteristics were used to avoid over-fitting. Selection of these two spatial  
261 characteristics were based on a Spearman correlation analysis between the fitted parameter values of  
262 each temporal predictor variable and the fifty potential spatial explanatory variables (as mentioned  
263 earlier in this section), following three steps:

- 264 1. from the 50 candidate spatial predictors, the one with the highest Spearman correlation with  $\beta T_N$  is  
265 selected as  $ST_{N1}$ , provided the correlation is statistically significant ( $p < 0.05$ );
- 266 2. the subset of remaining spatial predictors with spearman correlation with  $ST_{N1} < 0.7$  is found; and
- 267 3. from this subset, the spatial predictor with the highest spearman correlation with  $\beta T_N$  is selected as  
268  $ST_{N2}$ , provided the correlation has  $p < 0.05$ ;

269 Steps 2 and 3 intended to avoid cross-correlations between  $ST_{N1}$  and  $ST_{N2}$ . The selected spatial  
270 characteristics that influence the temporal relationships in our model are presented and interpreted in  
271 Section 3.1. Note that the entire process to select  $ST_{N1}$  and  $ST_{N2}$  was performed with the fitted  
272 parameters for each predictor of the temporal variability obtained from Guo et al. (2019).

#### 273 2.1.4 Model calibration

274 After identifying the spatial and temporal predictors for each constituent, as well as the spatial

275 characteristics which affect the strengths of each temporal predictor, the Bayesian hierarchical spatio-  
276 temporal model was fitted for each constituent across all monitoring sites simultaneously. To achieve  
277 this, we used the R package *rstan* (Stan Development Team, 2018), which enabled both the sampling of  
278 parameter values from posterior distributions with Markov chain Monte Carlo (MCMC) and model  
279 evaluation. Constituent standard deviation ( $\sigma$ ) was assumed to be drawn from a minimally informative  
280 prior half-normal of  $N(0,10)$  distribution truncated to only positive values (Gelman, 2006; Stan  
281 Development Team, 2018). The regression coefficient of each spatial predictor ( $\beta S_1, \beta S_2, \dots, \beta S_m$  in Eq.  
282 3) was independently drawn from hyper-parameter distributions of  $N(\mu\beta S_M, \sigma\beta S_M)$ . The site-level  
283 regression coefficients of the temporal predictors ( $\beta T_{1,j}, \beta T_{2,j}, \dots, \beta T_{n,j}$  in Eq. 4, respectively) were  
284 sampled from the corresponding hyper-parameter distribution of  $N(\mu\beta T_N, \sigma\beta T_N)$ . The hyper-parameters  
285 were further assumed to be drawn from minimally informative prior distributions, following  
286 recommendations in Gelman (2006) and Stan Development Team (2019): for all the hyper-parameter  
287 means, a normal prior distribution of  $N(0,5)$  was used; for all the hyper-parameter standard deviations,  
288 a half-normal prior distribution of  $N(0,10)$  was used, which was truncated to only positive values. In  
289 each model run there were four independent Markov chains. A total of 20,000 iterations were used for  
290 each chain. Convergence of the chains was ensured by checking the *Rhat* value (Sturtz et al., 2005),  
291 which is a summary statistic on the convergence of the Bayesian models from the four Markov chains  
292 used in model calibration (Stan Development Team, 2018). Specifically, an *Rhat* value much greater  
293 than 1 indicates that the independent Markov chains have not been mixed well, and a value of below 1.1  
294 is recommended (Stan Development Team, 2018).

## 295 **2.2 Model performance evaluation and sensitivity analyses**

296 Performance evaluation of the model was undertaken on several aspects of the model results (Section.  
297 3.2). Since the model was calibrated in a Box-Cox transformation scale (see justification in Section  
298 2.1.2), the Box-Cox transformation scale was used for model evaluation to enable a clear investigation  
299 on the influences of a wide range of factors that can influence model performance. Detailed performance  
300 evaluations include:

- 301 1. *Ability to capture total spatio-temporal variability.* Firstly, the simulations from the fitted model  
302 and the corresponding observed concentrations were compared at 102 sites altogether to

303 understand how the overall spatio-temporal variabilities were captured. For each constituent,  
304 this evaluation was performed with: 1) these above-DL data to focus only on data used for  
305 calibration (as detailed in Section. 2.1.2); and 2) the full dataset including the below-DL data  
306 (set to half of the DL of the specific constituent), to understand how well the model represents  
307 the full distribution of constituent concentrations. A good model performance when including  
308 the below-DL data would suggest that the calibrated model is transferable to below-DL data  
309 too. All performance assessments were based on both visual inspection of model fitting as well  
310 as the Nash-Sutcliffe efficiency (NSE), which quantified the proportion of variability that was  
311 explained by the model (Nash and Sutcliffe, 1970).

312 2. *Proportions of spatial and temporal variability explained.* This involved a decomposition of the  
313 total observed variability using Eq. 2., into proportions contributed by spatial variability  
314 (variations in all site-mean concentrations from the grand average of site-mean concentrations)  
315 and temporal variability (variations in all concentrations from the corresponding site-mean  
316 concentrations). The corresponding modelled values were then used to calculate NSE for each  
317 variability component of each constituent.

318 3. *Ability to capture variation in ambient conditions across space, and temporal variation*  
319 *(including trends) across multiple catchments.* These were evaluated by a) comparing all  
320 simulated and observed site-averaged long-term mean concentrations; and b) comparing the  
321 simulated and observed time-series and long-term trends at representative sites. Further to a),  
322 performance was also evaluated on a real measurement scale by first back-transforming all  
323 modelled sample concentrations, calculating the back-transformed site-level means and then  
324 compared those to the corresponding observations. A further analysis to b) was also performed  
325 by comparing the estimated Sen's slope (Akritas et al., 1995) for the observations and  
326 simulations at all sites, and then computing the percentage of sites where the observed trends as  
327 indicated by the Sen's slope have been correctly represented by the model.

328 Additional evaluations of model sensitivity were conducted with calibration and validation on subsets  
329 of the full data (Section. 3.3), to understand model transferability and stability:

330 1. *Model sensitivity to the monitoring sites used for calibration.* We randomly selected 80% of the

331 sites for calibration and used the remaining 20% for validation, and repeated this validation  
332 process 50 times. We compared all calibration and validation performances of these ‘partial  
333 models’ with each other, as well as with the performance of the full model, to obtain a  
334 comprehensive evaluation of the sensitivity of model performance to calibration sites.

335 2. *Model sensitivity to calibration data period.* Since the study region was greatly influenced by a  
336 prolonged drought from 1997 to 2009 – known as the Millennium Drought (van Dijk et al.,  
337 2013), we also investigated model robustness for before, during and after this drought period.  
338 Specifically, we calibrated the model to each pre-, during- and post-drought period (1994-1996,  
339 1997-2009 and 2010-2014, respectively) with model validation on the remaining data. For  
340 example, when calibrating to the pre-drought period (1997-2009), validation was performed on  
341 the merged during and post-drought period (1994-1996 plus 2010-2014). The corresponding  
342 calibration and validation performances were compared with each other as well as against that  
343 of the full model, to identify potential impacts of the drought on model robustness.

### 344 3. Results

#### 345 3.1 Spatial variation in the impact of temporal factors

346 The key controls of the spatial and temporal variations in water quality have been identified in our two  
347 preceding studies (Lintern et al. 2018b, Guo et al. 2019) and briefly summarized in Section 2.1.3. and  
348 are thus not discussed here. As also detailed in Section 2.1.3, to achieve full spatio-temporal predictive  
349 capacity, the model developed in this study considers the spatial variation in the strength of each  
350 temporal predictor by using two additional catchment spatial characteristics ( $ST_{N1,j}$  and  $ST_{N2,j}$  in Eq.  
351 6). on the Spearman’s correlations. Here we focus on the most important temporal predictor for each  
352 constituent, streamflow, where Table 2 shows the two spatial characteristics identified that are most  
353 closely related to the spatial variation of the effects of impact of streamflow on water quality. The full  
354 list of the selected key catchment characteristics for all temporal predictors of each constituent is  
355 summarized in Table S5 and visualized in Figure S4.

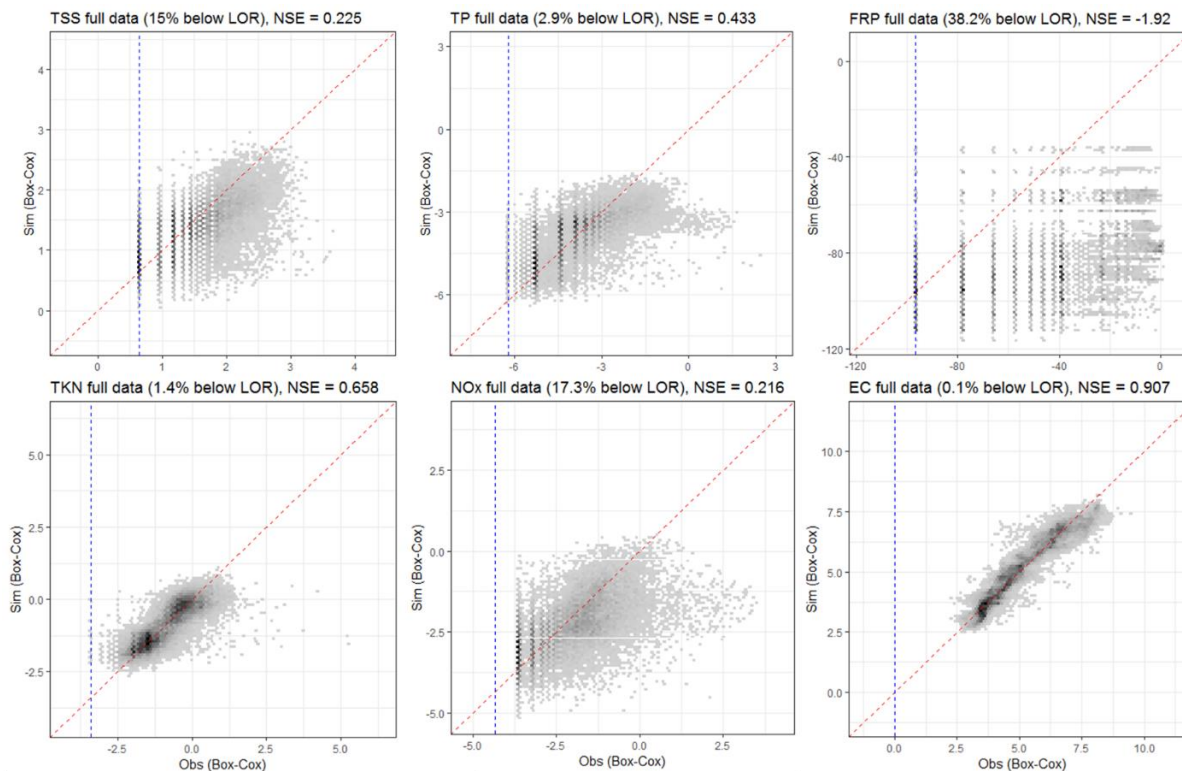
356 **Table 2. The key catchment landscape characteristics that are related to the varying relationships of water**  
357 **quality and same-day streamflow across space, which were selected as the two predictors for the**  
358 **streamflow effect in our model. The corresponding Spearman’s correlation ( $\rho$  at  $p < 0.05$ ) between the**  
359 **effect of streamflow and each catchment characteristic is presented.**

360 TSS, TP and TKN show consistent patterns of the spatial variation in the effects of streamflow on water

361 quality, which are strongly driven by the differences in average rainfall conditions across catchments.  
362 Specifically, streamflow generally has a larger effect on water quality in catchments with higher average  
363 annual rainfall. Since the streamflow effects are positive for the majority of catchments (as shown in  
364 Figure S5), these correlations indicate that for the same increase in transformed streamflow, a greater  
365 increase in transformed concentrations of TSS, TP and TKN will occur at a catchment with higher annual  
366 average rainfall. Given that the Box-Cox lambda values (Table S4) are close to zero, the transformation  
367 is log-like and hence changes in transformed flow and concentration approximately correspond to  
368 proportional changes in the real values of flow and concentration. In contrast, for FRP, NO<sub>x</sub> and EC, the  
369 spatial patterns of streamflow effects are specific to each constituent. This difference in the model results  
370 between TSS, TP and TKN against the other constituents might be related to the distinct transport  
371 pathways of particulate and dissolved constituents. The former is predominantly related to surface flow  
372 and thus relies heavily on rainfall contribution. Dissolved constituents are likely transported along the  
373 subsurface pathway. Apart from streamflow, the spatial patterns in other key temporal drivers of water  
374 quality (e.g. antecedent streamflow, soil moisture etc.) are less consistent across different constituents  
375 (Figure S4).

### 376 **3.2 Model performance evaluation**

377 The spatio-temporal water quality models show varying performances between the constituents. When  
378 assessed with only the above-DL data (Fig. 2), the best performing models are those for EC and TKN,  
379 which capture 90.7% and 65.8% of the total observed spatio-temporal variability. The modelling  
380 performance is lowest for FRP, NO<sub>x</sub> and TSS, with NSE values of -1.92, 0.216 and 0.225, respectively.  
381 When evaluated against the entire dataset (i.e., including both below- and above DL data), the models  
382 explain 19.9% (FRP) to 88.6% (EC) of spatio-temporal variability (Table 3). Model performances for  
383 FRP, NO<sub>x</sub> and TSS improve notably compared with the previous evaluation of above-DL data, however,  
384 they remain as the three constituents that are most difficult to predict. We further discuss the possible  
385 factors influencing their model performance in Section 4.1.



386

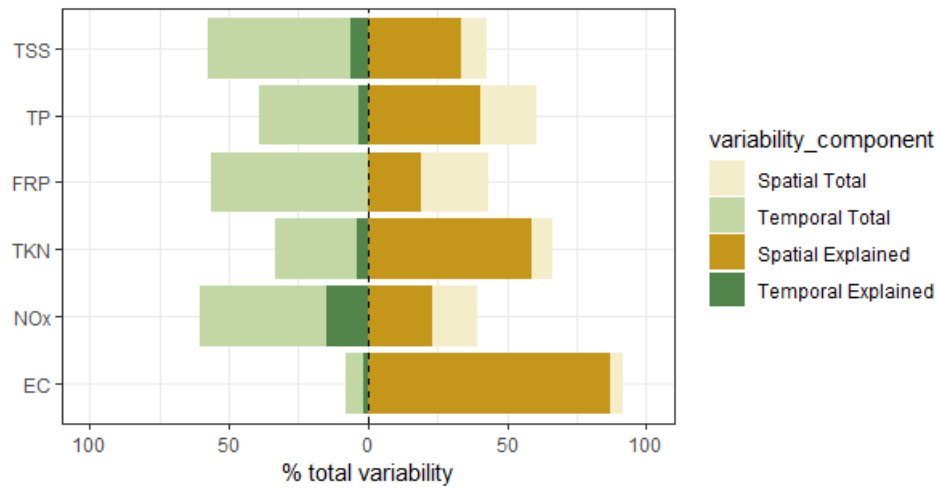
387 **Figure 2. Performance of the spatio-temporal models for each of the six constituents,**  
 388 **represented by the simulated median concentrations and corresponding observations of above-**  
 389 **DL records across all 102 calibration sites, in Box-Cox transformed space. Darker regions**  
 390 **represent denser distribution of simulation and observation points. Dashed red lines show the**  
 391 **1:1 lines whereas dashed blue lines show the DL levels. For each constituent, the percentage of**  
 392 **data below the DL and the model performance (NSE) are also specified.**

393 **Table 3. Comparison of model performance for all records and only the above-DL records for**  
 394 **each constituent.**

395 The model performance to predict spatial and temporal variability is summarized in Figure 3, which  
 396 compares the observed and explainable variability for each of the spatial and temporal components  
 397 (detailed in Section 2.1.4). Regarding the observed variability (lighter colours), EC is strongly  
 398 dominated by spatial variability (91.8%), highlighting that within-site variation in water quality is  
 399 minimal compared to between-site variation. To a lesser extent, spatial variability also contributes to  
 400 major proportions of total variability for TP and TKN (60.8% and 66.6%, respectively). TSS, FRP and  
 401 NO<sub>x</sub> are more influenced by temporal variability (57.4%, 56.6%, 60.5%, respectively).

402



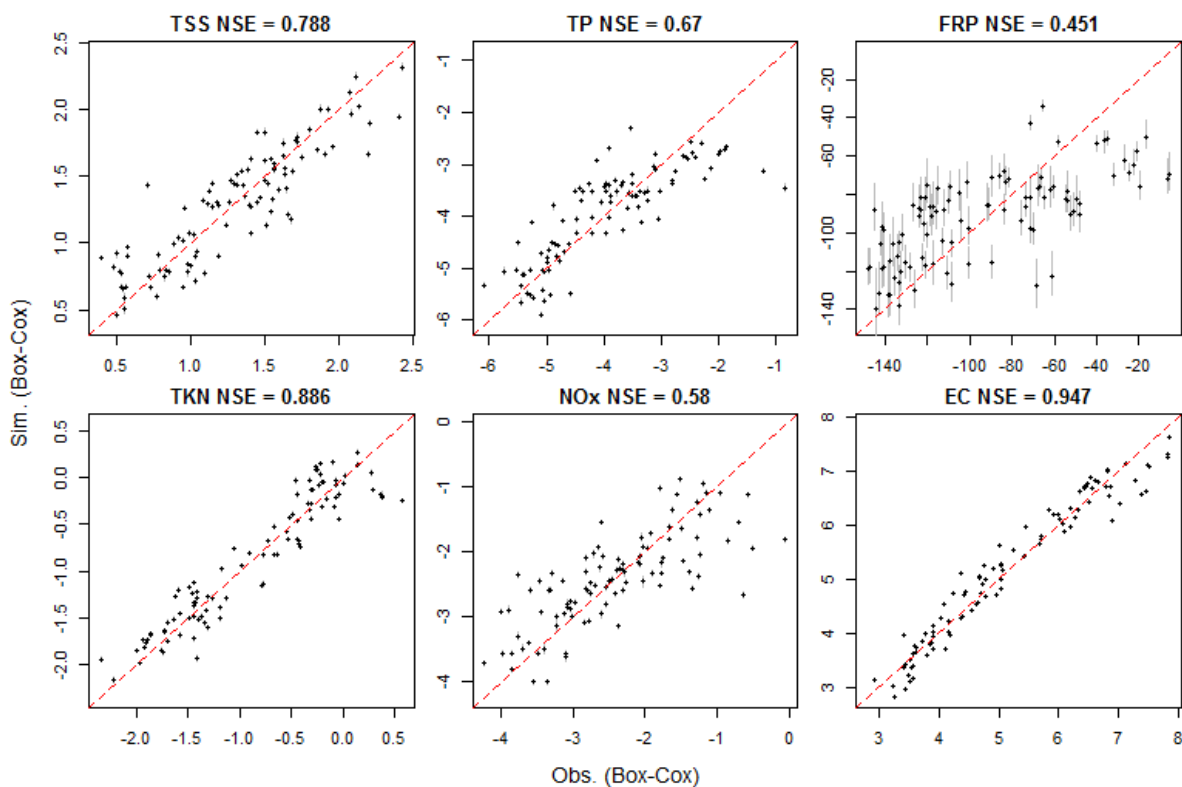


403

404 **Figure 3. Observed spatial and temporal variabilities as proportions of the total variability (total**  
 405 **width of each bar, 100%). The dashed line differentiates temporal variability (left side) with**  
 406 **spatial variability (right side), and the darker colours highlight the proportions of spatial and**  
 407 **temporal variabilities that are explainable by the model. All values were estimated in Box-Cox**  
 408 **transformed space.**

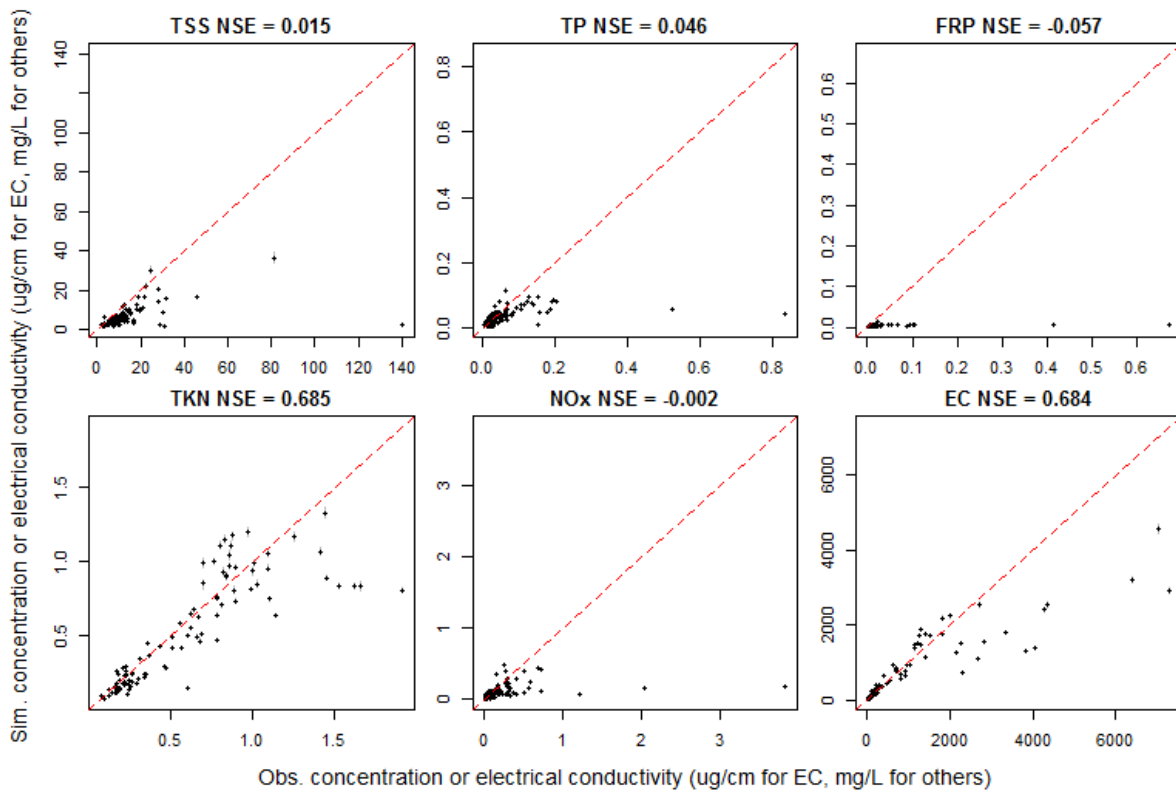
409 The explained variability (darker colours) show that, across all catchments, temporal variability is much  
 410 more difficult to model compared with spatial variability. It also appears that a substantial part of the  
 411 model's overall performance is driven by its ability to capture spatial variability in ambient water quality  
 412 conditions. For example, the models for TSS, FRP and NO<sub>x</sub> show poorer overall performance (Fig. 2,  
 413 with NSE values of 0.225, -1.92 and 0.216, respectively)), because the total variability for each of these  
 414 is dominated by temporal variability (57.4%, 56.6%, 60.5%, respectively), which largely remains  
 415 unexplained by the model (Fig. 3). In contrast, the EC model shows a very good fit with 90.7% of total  
 416 variability explained – 91.8% of the total observed variability is due to spatial variability, of which  
 417 94.7% is explained by the model. Therefore, although the EC model can only explain a small portion of  
 418 temporal variability (20% out of 8.2% of total variability), the overall model performance remains high.  
 419 As highlighted in Fig. 3, the model has good capacity to capture spatial variability in water quality. This  
 420 is further evaluated in Fig. 4 by comparing the simulated and observed site-level mean concentrations.  
 421 The highest model performance is for EC and lowest performance is for FRP (explaining 94.7% and  
 422 44.2% spatial variability, respectively). At the back-transformed scale, the model shows greater biases  
 423 for sites with higher concentrations (approximately the highest 10% sites for each constituent) (Fig. 5).  
 424 This is not surprising as the model was fitted to a Box-Cox transformed space that reduces focus on high  
 425 values and increases the focused on low values. This compromised its ability to represent sites with

426 unusually high concentrations. The implications of the model having higher predictive capacity in the  
427 transformed scale is further discussed in Section. 4.1.



428  
429 **Figure 4. Model fit for site-level mean concentration at the 102 calibration sites for six**  
430 **constituents, with the 95% lower and upper bounds of posterior simulations shown in vertical**  
431 **grey lines. All simulations and observations are presented in in Box-Cox transformed space. The**  
432 **NSE for each constituent is also shown and red dash lines show the 1:1 lines.**

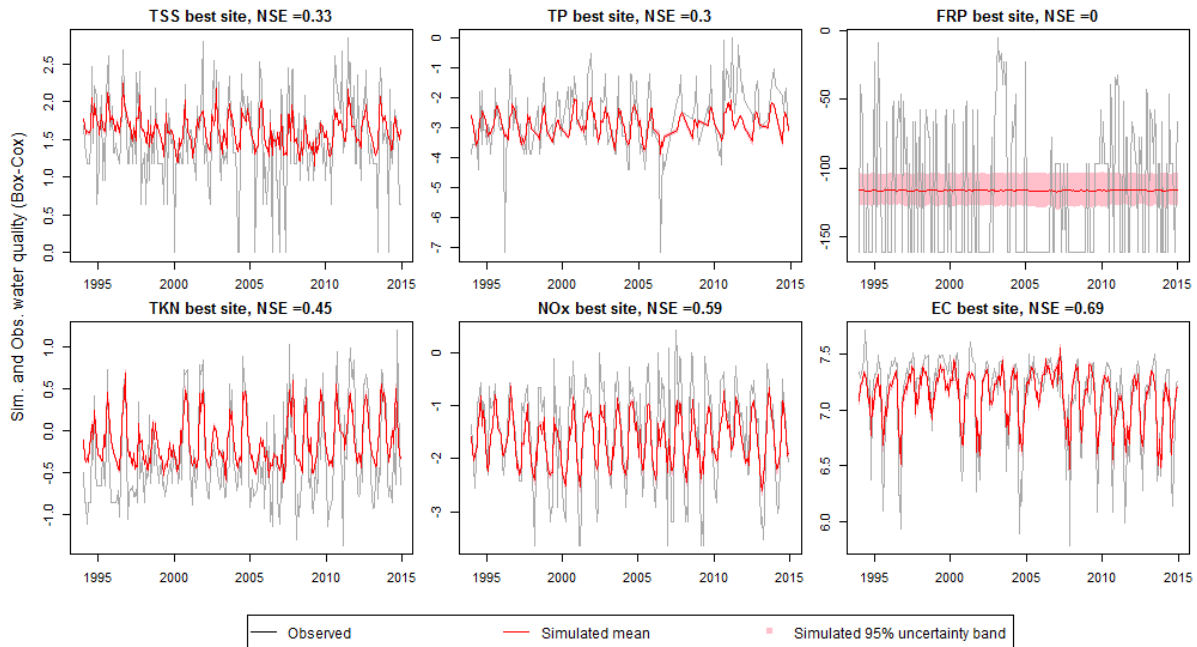
433



434

435 **Figure 5. Back-transformation of the model simulations to the measurement scale emphasizes lack of fit**  
 436 **for the highest concentrations, illustrated by simulated against observed site-level mean concentrations of**  
 437 **each constituent in a back-transformed scale. The 95% lower and upper bounds of all posterior**  
 438 **simulations shown in vertical grey lines. The NSE for each constituent is also shown and red dash lines**  
 439 **show the 1:1 lines.**  
 440

441 As also noted in Fig. 3, the ability of the spatio-temporal model to explain temporal variability remains  
 442 relatively limited. This is further explored in Fig. 6, where the observed and simulated time-series are  
 443 presented for one monitoring site for each constituent, at which the model performance (NSE) was the  
 444 highest. These results show that even for catchments where the model has the highest ability to capture  
 445 temporal variability, the model consistently underestimated temporal variability for all constituents.



446

447 **Figure 6. Model fit of the within-site (temporal) water quality variability, illustrated with the**  
 448 **observed and simulated time-series for the best-performing site for each constituent. All values**  
 449 **are presented in Box-Cox transformed space. The NSE for each constituent is also shown. The**  
 450 **red line indicates the corresponding mean of all posterior simulations, while the pink bands**  
 451 **show the corresponding 95% lower and upper bounds (only visible for FRP).**

452 Fig. 6 also illustrates that, although the model shows substantial underestimation of temporal variability  
 453 within site, long-term temporal trends in the time-series are well captured at the best sites (except for  
 454 FRP). Table 4 summarizes the ability of the model to capture observed trends across all 102 catchments  
 455 for each constituent. In general, the model is able to capture observed trends in most sites for NO<sub>x</sub> and  
 456 EC and for both positive and negative trends. For TP and TKN, positive trends are well captured while  
 457 for TSS the negative trends are better captured.

458 **Table 4. Model ability to capture observed water quality trends across all monitoring sites for**  
 459 **each constituent. The percentages of sites where observed positive and negative trends are**  
 460 **captured by the model are presented separately. Values in brackets indicate numbers of sites**  
 461 **where corresponding positive or negative trends are observed. For detailed estimation of these**  
 462 **percentages please refer to Sect. 2.2.**

### 463 3.3 Model sensitivity analyses

464 We first compare the performance of each spatio-temporal model fitted with the full dataset with those  
 465 obtained from the 50 corresponding “partial” models that were calibrated to only 80% of the monitoring  
 466 sites. Note that in this comparison, the FRP model was not assessed due to its poor performance (Section  
 467 3.2). The calibration and validation results for the 50 partial models are summarized in Table 5 along

468 with the performance of the full model calibrated to all 102 sites (see Figs. S6 and S7 in the  
469 Supplementary Material for detailed comparison of model residuals of the partial calibration/validation).  
470 Across constituents, the calibration performance of the full model was comparable with the 50 partial  
471 models. Note the slightly higher calibration performance for the partial models of NO<sub>x</sub> compared to the  
472 full model. This seems to be related to the generally lower percentages of below-DL data in the 50  
473 randomly-chosen partial calibration datasets (14.1%-17.9%) compared to the full dataset (17.3%) – we  
474 further discuss the impacts of below-DL data on model performance in Section 4.1. In addition, model  
475 performance is highly consistent between corresponding calibration and validation, with most  
476 differences in NSEs less than 0.1. These suggest that the spatio-temporal model performance is highly  
477 robust and unaffected by the choice of calibration sites.

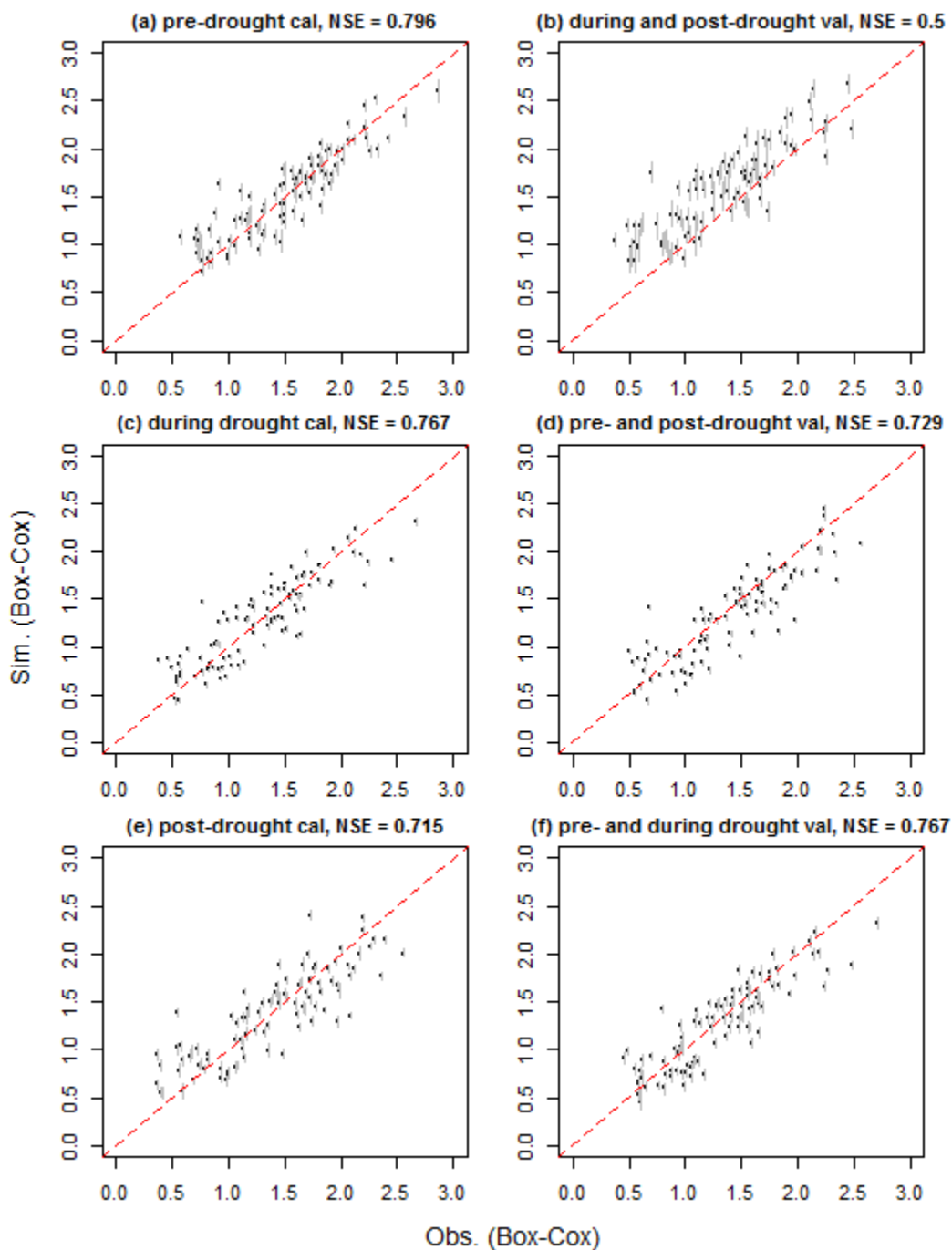
478 **Table 5. Comparison of model performances (as NSE) of the full model (Column 2) and the 50**  
479 **partial models (Columns 3 to 5) with each calibrated to 80% randomly selected monitoring sites.**  
480 **Columns 3 to 5 summarize the mean, minimum and maximum NSE values across the 50 runs,**  
481 **where for each constituent, the top row showing calibration performance and the bottom row**  
482 **showing the validation performance (i.e. at the 20% sites that were not used for calibration).**  
483

484 The performance of the full model for each constituent is also compared with that of the three models  
485 calibrated to the pre-, during and post-drought periods. In general, we observe consistent performance  
486 for each constituent, across calibrations to the three periods of contrasting hydrological conditions  
487 (Table 6, see Figs. S8 to S13 in the Supplementary Material for detailed model fittings). One notable  
488 common pattern is that the performance for calibration and validation is more consistent during the  
489 drought period than either the pre- and post-drought periods. However, this is most likely explained by  
490 relative sizes of the calibration data sets, which are 3, 13 and 5 years for the pre-, during and post-  
491 drought periods respectively.

492 Of all constituents (excluding FRP), TSS shows greater differences in model performances across  
493 periods – especially when comparing the pre-drought calibration with its validation for the site-level  
494 mean concentrations (Fig. 7). Notably, when calibrated to the pre-drought period and validated on both  
495 the during- and post-drought periods, the validated model over-estimates most of the data (Fig. 7 (b));

496 and when calibrated to the during-drought period, the validated model slightly under-estimates pre-  
497 and post-drought period TSS (Fig. 7 (d)).

498 **Table 6. Comparison of model performances (as NSE) of the full model and the three models**  
499 **that were calibrated to the pre-drought (1994-1996), drought (1997-2009) and the post-drought**  
500 **(2010-2014) periods. For each of the models, the calibration performance is shown on the top**  
501 **row and the validation performance (i.e. over the periods that were not used for calibration) is**  
502 **shown on the bottom row. See Section 2.1.4 for details of the calibration and validation**  
503 **approach.**

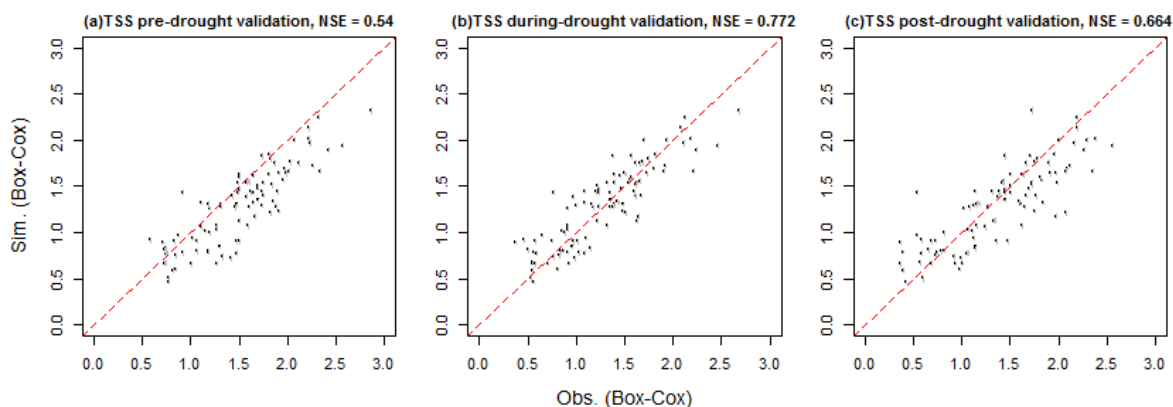


504 **Figure 7. Comparison of the TSS model performance, as the simulated against observed site-**  
505 **level mean concentrations in Box-Cox transformed space. The left column shows calibration**  
506 **performance for the model calibrated to the pre-drought (1994-1996), drought (1997-2009) and**  
507 **the post-drought (2010-2014) periods, respectively; the right column shows the corresponding**  
508

509 validation performance for each period. The 95% lower and upper bounds of simulations shown  
510 in vertical grey lines and red dash lines show the 1:1 lines.  
511

512 The potential impacts of drought on TSS dynamics are further illustrated with the performance of the  
513 spatio-temporal model (calibrated to the full dataset with all sites and all data from 1994 to 2014) over  
514 the pre-, during and post-drought periods (Fig. 8). Both the during- and post-drought periods have  
515 consistently good performances, while the model underestimates most sites for the pre-drought period.  
516 This is consistent with Fig. 7 in suggesting a systematic decrease in TSS concentration since the drought  
517 began. The better performance of the full model during and after drought (Fig. 8) can be a result of the  
518 calibration period of the full spatio-temporal model – between 1994 and 2014 – which was dominated  
519 by the during- and post-drought periods.

520 In summary, Figs 7 and 8 together with Figs. S13-S17 suggest that whilst model performance for most  
521 constituents are not affected by the hydrological periods used for calibration and validation, the  
522 calibration period did have notable impact on TSS. Some possible causes are discussed in Section 4.3.



523  
524 **Figure 8. Comparison of the performance of the full spatio-temporal TSS model calibrated to all**  
525 **data across a) pre-drought (1994-1996), b) during drought (1997-2009) and c) post-drought**  
526 **(2010-2014) periods, as represented by the simulated against observed site-level mean**  
527 **concentrations in Box-Cox transformed space. The 95% lower and upper bounds of simulations**  
528 **shown in vertical grey lines and red dash lines show the 1:1 lines.**

## 529 4. Discussion

### 530 4.1 Implications for statistical water quality modelling

531 In this study, we developed the first process-informed statistical model that is capable of explaining a  
532 reasonable proportion of water quality variability for a large spatial area of over 130,000km<sup>2</sup>. Although  
533 the calibration data have relatively low sampling frequency (i.e. monthly), our model generally performs

534 satisfactorily in explaining the total variability in water quality. This demonstrates the effectiveness of  
535 the Bayesian hierarchical modelling framework in predicting spatio-temporal variability in water quality  
536 across large scales. The Bayesian hierarchical model is: a) more advantageous than other simpler  
537 statistical water quality models with its more comprehensive and process-informed approach, and  
538 capacity to represent varying temporal relationships across large-scale regions; b) less demanding for  
539 input data compared with those required by fully-distributed, processes-based models. From a practical  
540 perspective, this model has the potential to contribute to a number of management activities including  
541 catchment planning, management and policy-making activities, specifically:

- 542 1) The spatial predictive capacity can be used to identify pollution hot-spots and the catchment  
543 conditions that are likely causes of high concentrations. This can be used to help identify target  
544 catchment(s) to prioritize future water quality monitoring and management (Figs. 4 and 5);
- 545 2) Further to 1), since water quality has been linked with catchment characteristics in this model,  
546 it can also be used to assess potential impacts of alternative options of land use and land cover  
547 change, as well as potential effects of climate change, on ambient water quality conditions;
- 548 3) The model's temporal predictive capacity can identify changes in water quality due to changes  
549 in hydro-climatic conditions and vegetation cover, and thus enabling attribution of detected  
550 trends. On the other hand, any 'unexpected' trends can be identified to prompt further  
551 investigation to identify causes (Figure 6 and Table 4). The model could also be used for  
552 assessing the impacts of long-term catchment changes on water quality (Figures 7 and 8).

553 Despite the opportunities highlighted above, the model's performance also suggests some current  
554 limitations of the modelling framework in the following situations:

- 555 1) *High within-site temporal variability.* In Section 3.2 we have identified a general lack of  
556 predictive power for temporal variability. The potential impacts of high temporal variability on  
557 model performance is particularly evident for results of TSS, NO<sub>x</sub> and FRP in Fig. 3. Since our  
558 model has already included hydro-climatic conditions and vegetation cover to explain temporal  
559 variability, the unexplained temporal variability is likely due to other uncaptured temporal  
560 drivers. These could be: changes in land use and land management, bio-geochemical processes,



561 or transit time of water through catchments.

562 2) *Presence of high proportions of below-DL data.* The full datasets for the three poorly modelled  
563 constituents (FRP, TSS and NO<sub>x</sub>) all have higher proportions of data below the detection limit  
564 (38.2% 17.3% and 15% of all data, respectively) compared with other constituents. As  
565 illustrated in Fig. 2, for each of these constituents, removal of below-DL data before model  
566 calibration had created clear a truncation on the left-hand side of the distribution. This  
567 substantially increases the degrees of skewness and discontinuity of the data, essentially  
568 violating the assumption of normally distributed residuals and thus limiting model performance.  
569 The model capacity to handle truncated data might be improved by model fitting approaches  
570 explicitly designed for this issue. For example, Wang and Robertson (2011) and Zhao et al.  
571 (2016) illustrated an approach to resolving the discontinuity of the likelihood estimation in  
572 model fitting to data with presence of a lower bound such as zero rainfall values.

573 3) *Non-conservativeness of constituents.* The results indicate that the reactivity of the constituent  
574 is broadly associated with performance, which suggest that bio-geochemical processes (e.g.  
575 phosphorus cycling, nitrification/de-nitrification) can make water quality dynamics more  
576 difficult for the model to capture. To better capture changes in reactive constituents, the model  
577 may require greater consideration of and more extensive spatial and temporal data to represent  
578 bio-geochemical processes. Examples include improvements on the process representation for  
579 nitrogen cycling and the desorption and adsorption of phosphorus (Granger et al., 2010; Smyth  
580 et al., 2013; Tian and Zhou, 2007).

581 As previously noted, our model was developed in a Box-Cox transformed scale to ensure the validity of  
582 the statistical assumptions (see details on data transformation in Sect. 2.1.2), which shows limited  
583 performance for high constituent concentrations when simulations are back-transformed to the  
584 measurement scale (Figs. 4 and 5). However, our model approximately represents proportional changes  
585 in water quality<sup>1</sup>, which can thus help managers to understand proportional changes to inform practical  
586 catchment management.

587 For future implementations, the established model structure and parameterization would be best suited  
588 to within the study region. Before performing new simulations (e.g. for new monitoring sites or for  
589 current study sites over a different time-period), the statistical properties of the new input datasets should  
590 be checked to ensure that they are similar to the calibration datasets. To model new catchments outside  
591 of the study region, a re-calibration of the model is required. This would involve extensive selection of  
592 key predictors and model calibration, much as performed in this study and the two preceding ones  
593 (Lintern et al., 2018b; Guo et al., 2019). A sufficiently long record length (e.g. 20 years) is ideal for such  
594 modelling, as it ensures a reasonable understanding of the temporal variability to be obtained.

#### 595 **4.2 Implications for water quality monitoring programs**

596 The current spatio-temporal model extracts water quality temporal variability from monthly data.  
597 Utilizing data with higher temporal resolution may further strengthen the model capacity to explain  
598 temporal variability, especially by capturing more information on water quality dynamics during flow  
599 events. This may be possible into the future; however, current high-frequency water quality sensors  
600 (Bende-Michl and Hairsine, 2010; Outram et al., 2014; Lannergård et al., 2019; Pellerin et al., 2016) still  
601 have very high resourcing requirements that limits widespread deployment in operational networks.

602 Furthermore, changes in land use and management over time are currently not considered here as  
603 predictors of temporal variability in water quality, which include but not limit to land clearing,  
604 urbanization, tillage, fertiliser application and irrigation. This is due to a complete lack, or inconsistency  
605 of available data. However, changes in land use/land management practices can occur over short time  
606 periods, which can lead to increases in pollutant sources and changes to runoff generation processes  
607 (e.g. Tang et al., 2005; DeFries and Eshleman, 2004; Smith et al., 2013). Therefore, our modelling

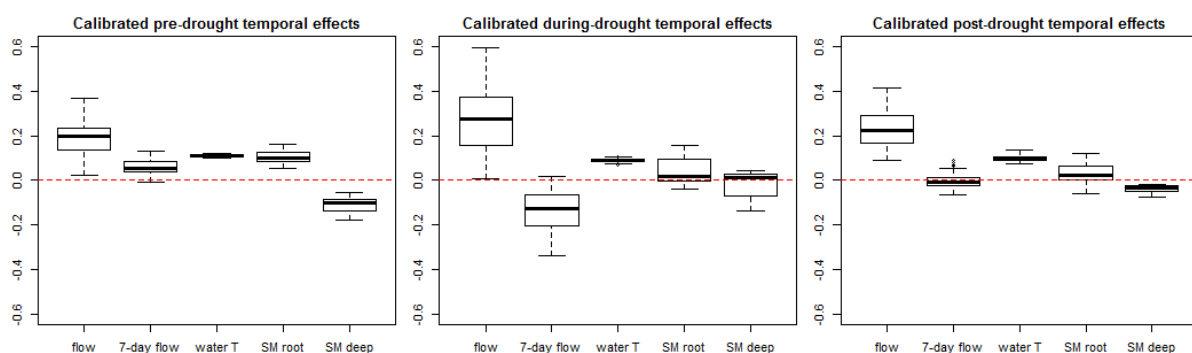
<sup>1</sup>All Box-Cox transformation parameters for water quality constituents are approximately 0 (Table S4), which means that the transformations are similar to a log transformation.

608 framework can potentially be improved by having additional monitoring data on the temporal patterns  
609 of land use/land management to better capture their impacts on water quality.

#### 610 4.3 Potential impacts of long-term drought on water quality dynamics

611 Results of model calibration and validation to different time periods suggest a systematic decrease in  
612 TSS concentrations during and after the prolonged drought, in comparison with the pre-drought period  
613 under the same spatial and temporal conditions. Such a shift is not observed for any other five  
614 constituents analyzed (nutrients and salts) (Section 3.3).

615 A further analysis of the calibrated model parameters for pre-, during and post-drought periods suggest  
616 that the effects of key spatial predictors do not vary much across periods (Figure S14). In contrast, the  
617 effects of key temporal predictors highlight a clear shift in the role of antecedent flow (prior 7-day flow)  
618 across different time periods (Figure 9). Specifically, the antecedent flow effects are mostly positive  
619 across catchments before the drought, and shift to mostly negative during the drought. After the drought,  
620 the antecedent flow effects have mixed directions among different catchments. Considering the limited  
621 performance of the TSS model (i.e. substantial under-estimation of temporal variability in Section 3.1),  
622 these changing relationships suggested in the calibrated parameters might be unreliable. However, this  
623 should not affect the reliability of the observed change in TSS since the drought (Section 3.3), which  
624 was based on the systematic differences of model fitting between different periods, revealing a broad-  
625 scale patterns across the state on the drought influences.



626  
627 **Figure 9. Effects of the five key predictors for the temporal variability in TSS across 102 sites,**  
628 **summarized by the posterior mean of the calibrated parameter values for each predictor (box**  
629 **shows values across all sites), from left: flow, 7-day antecedent flow, water temperature, root-**  
630 **zone soil moisture and deep soil moisture.**

631 In the literature, impacts of the Millennium Drought on the hydrology and runoff regimes of south-  
632 eastern Australia are well understood (van Dijk et al., 2013; Leblanc et al., 2012; Saft et al., 2015).

633 However, less is known about how this major and prolonged drought event has impacted water quality  
634 (Bond et al., 2008). Previous studies on other drought events around the world mainly focused on  
635 changes in water quality as responses to the reduced streamflow during drought. For example, reduction  
636 in sediment levels during drought has been reported and attributed to lower erosion from the contributing  
637 catchment, together with lower rates of solid transport associated with reduced flows (Murdoch et al.,  
638 2000;Caruso, 2002). At a more local scale, increasing sediment concentrations during drought have also  
639 been observed in streams adjacent to land with high densities of livestock and bushland, which both  
640 constantly contribute to sediment load during drought, leading to elevated concentrations with lower  
641 dilution rate (Caruso, 2002). Similar to sediments, the impact of droughts on stream nutrient and salt  
642 concentrations have also commonly been understood as responses to reduced runoff generation and  
643 streamflow. In catchments with no significant point-source pollution, nutrient concentrations typically  
644 decreased during droughts (Mosley, 2015) with less nutrient leaching and overland flow, but may also  
645 increase due to increasing livestock inputs at more local scales (Caruso, 2002). In contrast, catchments  
646 with significant point-source pollution generally experience water quality deterioration during drought  
647 due to reduced dilution (van Vliet and Zwolsman, 2008;Mosley, 2015). For salinity, concentration often  
648 increases during drought with reduced dilution and increased evaporation (Caruso, 2002). This is  
649 particularly evident for catchments that are more influenced by saline groundwater input as the relative  
650 contribution of groundwater increased during drought (Costelloe et al., 2005).

651 In contrast to these previous studies, our findings suggest additional possible pathways along which  
652 drought can affect stream water quality, that prolonged drought might have altered the relationships  
653 between sediments and its predictors (Figs. 7 and 8). In contrast to sediments, our model suggests no  
654 clear shifts in the dynamics of nutrients and salts in a regional scale. Our findings are in line with a few  
655 previous studies which reported temporal changes in the concentration-discharge relationships for  
656 sediments and nutrients, specifically, when comparing high- and low-flow conditions (Zhang,  
657 2018;Moatar et al., 2017), as well as drought and recovery period (Burt et al., 2015). Our findings  
658 provide extra dimensions to what would be offered by simple trend analyses using approaches such as  
659 Mann Kendall test or Sen's slope (e.g. Smith et al., 1987;Chang, 2008;Hirsch et al., 1991;Bouza-Deaño  
660 et al., 2008). Those approaches are only capable of indicating direction and magnitude of observed

661 trends. In contrast, our model was able to attribute the consistent upward shift in TSS concentration to  
662 change in relationships between water quality and its key driving factors since the start of drought.

663 In addition, we also acknowledge that our ability to represent the pre- and post-drought conditions in  
664 this study may be limited by the record length, since only 2 years of pre-drought and 4 years of post-  
665 drought data were available. Once longer records build up, they will enable us to update our  
666 understanding of the impact of this prolonged drought. We would be also able to conduct more  
667 sophisticated investigations, such as comparing the impacts of long-term droughts versus individual dry  
668 and wet years and events (e.g. Saft et al., 2015; Outram et al., 2014; Burt et al., 2015).

## 669 **5. Conclusions**

670 This study aims to address the current lack of water quality models that operate at large scales across  
671 multiple catchments. To achieve this, we used long-term stream water quality data collected from 102  
672 sites in south-eastern Australia, and developed a Bayesian hierarchical statistical model to simulate the  
673 spatio-temporal variabilities in six key water quality constituents: TSS, TP, FRP, TKN, NO<sub>x</sub> and EC.  
674 The choice of model predictors was guided by previous studies on the same dataset (Lintern et al.,  
675 2018b; Guo et al., 2019). The model generally well captures the spatio-temporal variability in water  
676 quality, where spatial variability between catchments is much better represented than temporal  
677 variability. The model is best used to predict proportional changes in water quality in a Box-Cox  
678 transformed scale, and can have substantial bias if used to predict absolute values for high  
679 concentrations. Cross-validation shows that the spatio-temporal model can predict water quality in non-  
680 monitored locations under similar conditions to the historical period and the calibration catchments that  
681 we investigated. This can assist management by (1) identifying hot-spots and key temporal periods for  
682 waterway pollution; (2) testing effects of catchment changes e.g. urbanization or afforestation; and (3)  
683 identifying and attributing major water quality trends and changes.

684 Based on the above model evaluations, we discussed potential ways to further enhance the model  
685 performance. In improving the modelling framework, alternative statistical approaches could be  
686 considered to reduce the impact of below detection limit data on model performance. In addition, the  
687 models could be extended to consider some key bio-geochemical processes to better dynamics in non-  
688 conservative constituents (e.g., FRP or NO<sub>x</sub>). Regarding data availability, the current models could

689 potentially benefit from improved monitoring of changes in land use intensity and management to be  
690 able to include these drivers in the model. The inclusion of high-frequency water quality sampling data  
691 may also extend the model's ability to represent temporal variability. However, high-frequency water  
692 quality data are also typically highly variable with large noise. Therefore, the implication of such data  
693 for the spatio-temporal modelling framework remains an open question, which needs further  
694 investigation in future applications of this modeling framework.

### 695 **Data availability**

696 All data used in this study were extracted from public domain. All stream water quality data were  
697 extracted from the Victorian Water Measurement Information System (via <http://data.water.vic.gov.au/>,  
698 provided by the Department of Environment Land Water and Planning Victoria). The catchments  
699 corresponding to these water quality monitoring sites were delineated using the Geofabric tool provided  
700 by the Bureau of Meteorology, via <ftp://ftp.bom.gov.au/anon/home/geofabric/>. We have listed the  
701 sources of all other data for the spatial and temporal predictors of our models in Tables S1 and S2 in the  
702 Supplementary Materials.

### 703 **Author contribution**

704 All authors contributed to the conceptualization the models and the design of methodology. A. Lintern  
705 and S. Liu contributed to the data curatiom. D.Guo carried out the formal analyses, visualization and  
706 validation. J.A. Webb, D. Ryu, U. Bende-Michl and A.W. Western contributed to the funding  
707 acquisition. D. Guo, A. Lintern, J.A. Webb, D. Ryu, S. Liu and A.W. Western contributed to the  
708 investigation. D. Guo carried out project administration and coding to run the experiments. J.A. Webb,  
709 D. Ryu, and A.W. Western contributed to the supervision. D.Guo prepared the manuscript with  
710 contributions from all co-authors.

### 711 **Competing interests**

712 The authors declare that they have no conflict of interest.

### 713 **Acknowledgement**

714 The Australian Research Council, the Victorian Environment Protection Authority, the Victorian

715 Department of Environment, Land Water and Planning, the Australian Bureau of Meteorology and the  
716 Queensland Department of Natural Resources, Mines and Energy provided funding for this project  
717 through the linkage program (LP140100495). The authors would also like to thank Matthew Johnson,  
718 Louise Sullivan, Hannah Sleeth and Jie Jian, for their assistance in the compilation and analysis of data.  
719 All water quality data used for this project can be found on: Water Measurement Information System  
720 (<http://data.water.vic.gov.au/monitoring.htm>). Sources of other data are provided in Tables S1 and S2  
721 of the Supplementary Materials.  
722

- 724 Abbaspour, K. C., Rouholahnejad, E., Vaghefi, S., Srinivasan, R., Yang, H., and Kløve, B.: A continental-  
725 scale hydrology and water quality model for Europe: Calibration and uncertainty of a high-resolution  
726 large-scale SWAT model, *Journal of Hydrology*, 524, 733-752,  
727 <https://doi.org/10.1016/j.jhydrol.2015.03.027>, 2015.
- 728 Adams, R., Arafat, Y., Eate, V., Grace, M. R., Saffarpour, S., Weatherley, A. J., and Western, A. W.: A  
729 catchment study of sources and sinks of nutrients and sediments in south-east Australia, *Journal of*  
730 *Hydrology*, 515, 166-179, <https://doi.org/10.1016/j.jhydrol.2014.04.034>, 2014.
- 731 Ahearn, D. S., Sheibley, R. W., Dahlgren, R. A., and Keller, K. E.: Temporal dynamics of stream water  
732 chemistry in the last free-flowing river draining the western Sierra Nevada, California, *Journal of*  
733 *Hydrology*, 295, 47-63, <https://doi.org/10.1016/j.jhydrol.2004.02.016>, 2004.
- 734 Ai, L., Shi, Z. H., Yin, W., and Huang, X.: Spatial and seasonal patterns in stream water contamination  
735 across mountainous watersheds: Linkage with landscape characteristics, *Journal of Hydrology*, 523,  
736 398-408, <https://doi.org/10.1016/j.jhydrol.2015.01.082>, 2015.
- 737 Akaike, H.: A new look at the statistical model identification, *IEEE transactions on automatic control*,  
738 19, 716-723, 1974.
- 739 Akritas, M. G., Murphy, S. A., and Lavalley, M. P.: The Theil-Sen estimator with doubly censored data  
740 and applications to astronomy, *Journal of the American Statistical Association*, 90, 170-177, 1995.
- 741 Ali, G., Wilson, H., Elliott, J., Penner, A., Haque, A., Ross, C., and Rabie, M.: Phosphorus export dynamics  
742 and hydrobiogeochemical controls across gradients of scale, topography and human impact,  
743 *Hydrological Processes*, 31, 3130-3145, 10.1002/hyp.11258, 2017.
- 744 Australian Water Technologies: Victorian water quality monitoring network and state biological  
745 monitoring programme manual of procedures, Australian Water Technologies, 68 Ricketts Rd, Mt  
746 Waverley VIC 3149, 1999.
- 747 Bailey, R. T., and Ahmadi, M.: Spatial and temporal variability of in-stream water quality parameter  
748 influence on dissolved oxygen and nitrate within a regional stream network, *Ecological modelling*, 277,  
749 87-96, 2014.
- 750 Bende-Michl, U., and Hairsine, P. B.: A systematic approach to choosing an automated nutrient  
751 analyser for river monitoring, *Journal of Environmental Monitoring*, 12, 127-134, 2010.
- 752 Bond, N. R., Lake, P. S., and Arthington, A. H.: The impacts of drought on freshwater ecosystems: an  
753 Australian perspective, *Hydrobiologia*, 600, 3-16, 10.1007/s10750-008-9326-z, 2008.
- 754 Borsuk, M. E., Higdon, D., Stow, C. A., and Reckhow, K. H.: A Bayesian hierarchical model to predict  
755 benthic oxygen demand from organic matter loading in estuaries and coastal zones, *Ecological*  
756 *Modelling*, 143, 165-181, [https://doi.org/10.1016/S0304-3800\(01\)00328-3](https://doi.org/10.1016/S0304-3800(01)00328-3), 2001.
- 757 Bouza-Deaño, R., Ternero-Rodríguez, M., and Fernández-Espinosa, A. J.: Trend study and assessment  
758 of surface water quality in the Ebro River (Spain), *Journal of Hydrology*, 361, 227-239,  
759 <https://doi.org/10.1016/j.jhydrol.2008.07.048>, 2008.
- 760 Box, G. E., and Cox, D. R.: An analysis of transformations, *Journal of the Royal Statistical Society: Series*  
761 *B (Methodological)*, 26, 211-243, 1964.
- 762 Bureau of Meteorology: Geofabric V2 2012.
- 763 Bureau of Rural Sciences: 2005/06 Land use of Australia, version 4. . 2010.
- 764 Burt, T. P., Worrall, F., Howden, N. J. K., and Anderson, M. G.: Shifts in discharge-concentration  
765 relationships as a small catchment recover from severe drought, *Hydrological Processes*, 29, 498-507,  
766 10.1002/hyp.10169, 2015.
- 767 Carey, R. O., and Migliaccio, K. W.: Contribution of wastewater treatment plant effluents to nutrient  
768 dynamics in aquatic systems: a review, *Environ Manage*, 44, 205-217, 10.1007/s00267-009-9309-5,  
769 2009.
- 770 Caruso, B. S.: Temporal and spatial patterns of extreme low flows and effects on stream ecosystems in  
771 Otago, New Zealand, *Journal of Hydrology*, 257, 115-133, [https://doi.org/10.1016/S0022-1694\(01\)00546-7](https://doi.org/10.1016/S0022-1694(01)00546-7), 2002.
- 773 Chang, H.: Spatial analysis of water quality trends in the Han River basin, South Korea, *Water Research*,  
774 42, 3285-3304, <https://doi.org/10.1016/j.watres.2008.04.006>, 2008.



775 Clark, J. S.: Why environmental scientists are becoming Bayesians, *Ecology Letters*, 8, 2-14,  
776 doi:10.1111/j.1461-0248.2004.00702.x, 2005.

777 Costelloe, J. F., Grayson, R. B., McMahon, T. A., and Argent, R. M.: Spatial and temporal variability of  
778 water salinity in an ephemeral, arid-zone river, central Australia, *Hydrological Processes*, 19, 3147-  
779 3166, 10.1002/hyp.5837, 2005.

780 DeFries, R., and Eshleman, K. N.: Land-use change and hydrologic processes: a major focus for the  
781 future, *Hydrological Processes*, 18, 2183-2186, doi:10.1002/hyp.5584, 2004.

782 Department of Environment Land Water and Planning Victoria: Victorian water measurement  
783 information system. . 2016.

784 Eidenshink, J. C.: The 1990 Conterminous U.S. AVHRR Data Set, *Photogrammetric Engineering and*  
785 *Remote Sensing*, 58, 1992.

786 Fraser, A. I., Harrod, T. R., and Haygarth, P. M.: The effect of rainfall intensity on soil erosion and  
787 particulate phosphorus transfer from arable soils, *Water Science and Technology*, 39, 41-45,  
788 [https://doi.org/10.1016/S0273-1223\(99\)00316-9](https://doi.org/10.1016/S0273-1223(99)00316-9), 1999.

789 Frost, A. J., Ramchurn, A., and Smith, A.: The bureau's operational AWRA landscape (AWRA-L) Model,  
790 Bureau of Meteorology, 2016.

791 Fu, B., Merritt, W. S., Croke, B. F. W., Weber, T., and Jakeman, A. J.: A review of catchment-scale water  
792 quality and erosion models and a synthesis of future prospects, *Environmental Modelling & Software*,  
793 <https://doi.org/10.1016/j.envsoft.2018.12.008>, 2018.

794 Gelman, A.: Prior distributions for variance parameters in hierarchical models (comment on article by  
795 Browne and Draper), *Bayesian Anal.*, 1, 515-534, 10.1214/06-BA117A, 2006.

796 Geoscience Australia: Dams and water storages. . 2004.

797 Geoscience Australia: Environmental Attributes Dataset. 2011.

798 Giri, S., and Qiu, Z.: Understanding the relationship of land uses and water quality in Twenty First  
799 Century: A review, *Journal of Environmental Management*, 173, 41-48,  
800 <https://doi.org/10.1016/j.jenvman.2016.02.029>, 2016.

801 Granger, S. J., Bol, R., Anthony, S., Owens, P. N., White, S. M., and Haygarth, P. M.: Chapter 3 - Towards  
802 a Holistic Classification of Diffuse Agricultural Water Pollution from Intensively Managed Grasslands  
803 on Heavy Soils, in: *Advances in Agronomy*, Academic Press, 83-115, 2010.

804 Guo, D., Lintern, A., Webb, J. A., Ryu, D., Liu, S., Bende-Michl, U., Leahy, P., Wilson, P., and Western, A.  
805 W.: Key Factors Affecting Temporal Variability in Stream Water Quality, *Water Resources Research*, 55,  
806 112-129, 10.1029/2018wr023370, 2019.

807 Heathwaite, A. L.: Multiple stressors on water availability at global to catchment scales: understanding  
808 human impact on nutrient cycles to protect water quality and water availability in the long term,  
809 *Freshwater Biology*, 55, 241-257, 10.1111/j.1365-2427.2009.02368.x, 2010.

810 Hirsch, R. M., Alexander, R. B., and Smith, R. A.: Selection of methods for the detection and estimation  
811 of trends in water quality, *Water Resources Research*, 27, 803-813, 10.1029/91wr00259, 1991.

812 Hrachowitz, M., Benettin, P., van Breukelen, B. M., Fovet, O., Howden, N. J. K., Ruiz, L., van der Velde,  
813 Y., and Wade, A. J.: Transit times—the link between hydrology and water quality at the catchment  
814 scale, *Wiley Interdisciplinary Reviews: Water*, 3, 629-657, doi:10.1002/wat2.1155, 2016.

815 Jarvie, H. P., Withers, J., and Neal, C.: Review of robust measurement of phosphorus in river water:  
816 sampling, storage, fractionation and sensitivity, *Hydrology and Earth System Sciences*, 6, 113-131, 2002.

817 Kingsford, R. T., Walker, K. F., Lester, R. E., Young, W. J., Fairweather, P. G., Sammut, J., and Geddes,  
818 M. C.: A Ramsar wetland in crisis – the Coorong, Lower Lakes and Murray Mouth, Australia, *Marine*  
819 *and Freshwater Research*, 62, 255-265, <https://doi.org/10.1071/MF09315>, 2011.

820 Kisi, O., and Parmar, K. S.: Application of least square support vector machine and multivariate adaptive  
821 regression spline models in long term prediction of river water pollution, *Journal of Hydrology*, 534,  
822 104-112, <https://doi.org/10.1016/j.jhydrol.2015.12.014>, 2016.

823 Kurunç, A., Yürekli, K., and Çevik, O.: Performance of two stochastic approaches for forecasting water  
824 quality and streamflow data from Yeşilırmak River, Turkey, *Environmental Modelling & Software*, 20,  
825 1195-1200, <https://doi.org/10.1016/j.envsoft.2004.11.001>, 2005.

826 Lannergård, E. E., Ledesma, J. L., Fölster, J., and Futter, M. N.: An evaluation of high frequency turbidity  
827 as a proxy for riverine total phosphorus concentrations, *Science of the Total Environment*, 651, 103-  
828 113, 2019.

829 Leblanc, M., Tweed, S., Van Dijk, A., and Timbal, B.: A review of historic and future hydrological changes  
830 in the Murray-Darling Basin, *Global and Planetary Change*, 80-81, 226-246,  
831 <https://doi.org/10.1016/j.gloplacha.2011.10.012>, 2012.

832 Lintern, A., Webb, J. A., Ryu, D., Liu, S., Bende-Michl, U., Waters, D., Leahy, P., Wilson, P., and Western,  
833 A. W.: Key factors influencing differences in stream water quality across space, *Wiley Interdisciplinary*  
834 *Reviews: Water*, 5, e1260, doi:10.1002/wat2.1260, 2018a.

835 Lintern, A., Webb, J. A., Ryu, D., Liu, S., Waters, D., Leahy, P., Bende-Michl, U., and Western, A. W.:  
836 What Are the Key Catchment Characteristics Affecting Spatial Differences in Riverine Water Quality?,  
837 *Water Resources Research*, doi:10.1029/2017WR022172, 2018b.

838 Luca Scrucca: Package 'GA', *The Comprehensive R Archive Network*, 2019.

839 May, R., Dandy, G., and Maier, H.: Review of input variable selection methods for artificial neural  
840 networks, in: *Artificial neural networks-methodological advances and biomedical applications*, InTech,  
841 2011.

842 Mellander, P.-E., Jordan, P., Shore, M., Melland, A. R., and Shortle, G.: Flow paths and phosphorus  
843 transfer pathways in two agricultural streams with contrasting flow controls, *Hydrological Processes*,  
844 29, 3504-3518, doi:10.1002/hyp.10415, 2015.

845 Meybeck, M., and Helmer, R.: The quality of rivers: From pristine stage to global pollution,  
846 *Palaeogeography, Palaeoclimatology, Palaeoecology*, 75, 283-309, [https://doi.org/10.1016/0031-  
847 0182\(89\)90191-0](https://doi.org/10.1016/0031-0182(89)90191-0), 1989.

848 Miller, C., Magdalena, A., Willows, R. I., Bowman, A. W., Scott, E. M., Lee, D., Burgess, C., Pope, L.,  
849 Pannullo, F., and Haggarty, R.: Spatiotemporal statistical modelling of long-term change in river  
850 nutrient concentrations in England & Wales, *Science of The Total Environment*, 466-467, 914-923,  
851 <https://doi.org/10.1016/j.scitotenv.2013.07.113>, 2014.

852 Moatar, F., Abbott, B. W., Minaudo, C., Curie, F., and Pinay, G.: Elemental properties, hydrology, and  
853 biology interact to shape concentration-discharge curves for carbon, nutrients, sediment, and major  
854 ions, *Water Resources Research*, 53, 1270-1287, 10.1002/2016wr019635, 2017.

855 Mosley, L. M.: Drought impacts on the water quality of freshwater systems; review and integration,  
856 *Earth-Science Reviews*, 140, 203-214, <https://doi.org/10.1016/j.earscirev.2014.11.010>, 2015.

857 Murdoch, P. S., Baron, J. S., and Miller, T. L.: POTENTIAL EFFECTS OF CLIMATE CHANGE ON SURFACE-  
858 WATER QUALITY IN NORTH AMERICA1, *JAWRA Journal of the American Water Resources Association*,  
859 36, 347-366, 10.1111/j.1752-1688.2000.tb04273.x, 2000.

860 Musolff, A., Schmidt, C., Selle, B., and Fleckenstein, J. H.: Catchment controls on solute export,  
861 *Advances in Water Resources*, 86, 133-146, <https://doi.org/10.1016/j.advwatres.2015.09.026>, 2015.

862 NASA LP DAAC: MOD13A3: MODIS/Terra Vegetation Indices Monthly L3 Global 1km V005. 2017.

863 Onderka, M., Wrede, S., Rodný, M., Pfister, L., Hoffmann, L., and Krein, A.: Hydrogeologic and  
864 landscape controls of dissolved inorganic nitrogen (DIN) and dissolved silica (DSi) fluxes in  
865 heterogeneous catchments, *Journal of Hydrology*, 450-451, 36-47,  
866 <https://doi.org/10.1016/j.jhydrol.2012.05.035>, 2012.

867 Outram, F. N., Lloyd, C. E. M., Jonczyk, J., Benskin, C. M. H., Grant, F., Perks, M. T., Deasy, C., Burke, S.  
868 P., Collins, A. L., Freer, J., Haygarth, P. M., Hiscock, K. M., Johnes, P. J., and Lovett, A. L.: High-frequency  
869 monitoring of nitrogen and phosphorus response in three rural catchments to the end of the 2011-  
870 2012 drought in England, *Hydrol. Earth Syst. Sci.*, 18, 3429-3448, 10.5194/hess-18-3429-2014, 2014.

871 Ouyang, W., Hao, F., Skidmore, A. K., and Toxopeus, A. G.: Soil erosion and sediment yield and their  
872 relationships with vegetation cover in upper stream of the Yellow River, *Science of The Total*  
873 *Environment*, 409, 396-403, <https://doi.org/10.1016/j.scitotenv.2010.10.020>, 2010.

874 Parmar, K. S., and Bhardwaj, R.: Statistical, time series, and fractal analysis of full stretch of river  
875 Yamuna (India) for water quality management, *Environmental Science and Pollution Research*, 22, 397-  
876 414, 10.1007/s11356-014-3346-1, 2015.

877 Pellerin, B. A., Stauffer, B. A., Young, D. A., Sullivan, D. J., Bricker, S. B., Walbridge, M. R., Clyde Jr., G.  
878 A., and Shaw, D. M.: Emerging Tools for Continuous Nutrient Monitoring Networks: Sensors Advancing

879 Science and Water Resources Protection, JAWRA Journal of the American Water Resources Association,  
880 52, 993-1008, 10.1111/1752-1688.12386, 2016.

881 Poor, C. J., and McDonnell, J. J.: The effects of land use on stream nitrate dynamics, Journal of  
882 Hydrology, 332, 54-68, <https://doi.org/10.1016/j.jhydrol.2006.06.022>, 2007.

883 Poudel, D. D., Lee, T., Srinivasan, R., Abbaspour, K., and Jeong, C. Y.: Assessment of seasonal and spatial  
884 variation of surface water quality, identification of factors associated with water quality variability, and  
885 the modeling of critical nonpoint source pollution areas in an agricultural watershed, Journal of Soil  
886 and Water Conservation, 68, 155-171, 10.2489/jswc.68.3.155, 2013.

887 Poulsen, D. L., Simmons, C. T., Le Galle La Salle, C., and Cox, J. W.: Assessing catchment-scale spatial  
888 and temporal patterns of groundwater and stream salinity, Hydrogeology Journal, 14, 1339-1359,  
889 10.1007/s10040-006-0065-9, 2006.

890 Qin, B., Zhu, G., Gao, G., Zhang, Y., Li, W., Paerl, H. W., and Carmichael, W. W.: A Drinking Water Crisis  
891 in Lake Taihu, China: Linkage to Climatic Variability and Lake Management, Environmental  
892 Management, 45, 105-112, 10.1007/s00267-009-9393-6, 2010.

893 Raupach, M., Briggs, P., Haverd, V., King, E., Paget, M., and Trudinger, C.: Australian water availability  
894 project (AWAP): CSIRO marine and atmospheric research component: final report for phase 3, 67, 2009.

895 Raupach, M., Briggs, P., Haverd, V., King, E., Paget, M., and Trudinger, C.: Australian Water Availability  
896 Project. CSIRO Marine and Atmospheric Research, Canberra, Australia., 2012.

897 Ren, W., Zhong, Y., Meligrana, J., Anderson, B., Watt, W. E., Chen, J., and Leung, H.-L.: Urbanization,  
898 land use, and water quality in Shanghai: 1947–1996, Environment International, 29, 649-659,  
899 [https://doi.org/10.1016/S0160-4120\(03\)00051-5](https://doi.org/10.1016/S0160-4120(03)00051-5), 2003.

900 Saft, M., Western, A. W., Zhang, L., Peel, M. C., and Potter, N. J.: The influence of multiyear drought on  
901 the annual rainfall-runoff relationship: An Australian perspective, Water Resources Research, 51, 2444-  
902 2463, doi:10.1002/2014WR015348, 2015.

903 Saft, M., Peel, M. C., Western, A. W., and Zhang, L.: Predicting shifts in rainfall-runoff partitioning  
904 during multiyear drought: Roles of dry period and catchment characteristics, Water Resources  
905 Research, 52, 9290-9305, doi:10.1002/2016WR019525, 2016.

906 Schwarz, G.: Estimating the dimension of a model, The annals of statistics, 6, 461-464, 1978.

907 Sharpley, A. N., Kleinman, P. J. A., McDowell, R. W., Gitau, M., and Bryant, R. B.: Modeling phosphorus  
908 transport in agricultural watersheds: Processes and possibilities, Journal of Soil and Water  
909 Conservation, 57, 425-439, 2002.

910 Smith, A. P., Western, A. W., and Hannah, M. C.: Linking water quality trends with land use  
911 intensification in dairy farming catchments, Journal of Hydrology, 476, 1-12, 2013.

912 Smith, R. A., Alexander, R. B., and Wolman, M. G.: Water-Quality Trends in the Nation's Rivers, Science,  
913 235, 1607-1615, 1987.

914 Smyth, A. R., Thompson, S. P., Siporin, K. N., Gardner, W. S., McCarthy, M. J., and Piehler, M. F.:  
915 Assessing nitrogen dynamics throughout the estuarine landscape, Estuaries and coasts, 36, 44-55, 2013.

916 Stan Development Team: RStan: the R interface to Stan. R package version 2.18.1, 2018.

917 Stan Reference Manual Version 2.20: [https://mc-stan.org/docs/2\\_20/reference-manual-2\\_20.pdf](https://mc-stan.org/docs/2_20/reference-manual-2_20.pdf),  
918 access: 28/09/2019, 2019.

919 Sueker, J. K., Clow, D. W., Ryan, J. N., and Jarrett, R. D.: Effect of basin physical characteristics on solute  
920 fluxes in nine alpine/subalpine basins, Colorado, USA, Hydrological Processes, 15, 2749-2769,  
921 10.1002/hyp.265, 2001.

922 Tang, Z., Engel, B. A., Pijanowski, B. C., and Lim, K. J.: Forecasting land use change and its environmental  
923 impact at a watershed scale, Journal of Environmental Management, 76, 35-45,  
924 <https://doi.org/10.1016/j.jenvman.2005.01.006>, 2005.

925 Terrestrial Ecosystem Research Network: Soil and landscape grid of Australia. 2016.

926 Tian, J. R., and Zhou, P. J.: Phosphorus fractions of floodplain sediments and phosphorus exchange on  
927 the sediment–water interface in the lower reaches of the Han River in China, Ecological Engineering,  
928 30, 264-270, <https://doi.org/10.1016/j.ecoleng.2007.01.006>, 2007.

929 Trambly, Y., Ouarda, T. B. M. J., St-Hilaire, A., and Poulin, J.: Regional estimation of extreme suspended  
930 sediment concentrations using watershed characteristics, Journal of Hydrology, 380, 305-317,  
931 <https://doi.org/10.1016/j.jhydrol.2009.11.006>, 2010.

932 van Dijk, A. I. J. M., Beck, H. E., Crosbie, R. S., de Jeu, R. A. M., Liu, Y. Y., Podger, G. M., Timbal, B., and  
933 Viney, N. R.: The Millennium Drought in southeast Australia (2001–2009): Natural and human causes  
934 and implications for water resources, ecosystems, economy, and society, *Water Resources Research*,  
935 49, 1040-1057, [10.1002/wrcr.20123](https://doi.org/10.1002/wrcr.20123), 2013.

936 van Vliet, M. T. H., and Zwolsman, J. J. G.: Impact of summer droughts on the water quality of the  
937 Meuse river, *Journal of Hydrology*, 353, 1-17, <https://doi.org/10.1016/j.jhydrol.2008.01.001>, 2008.

938 Varanka, S., Hjort, J., and Luoto, M.: Geomorphological factors predict water quality in boreal rivers,  
939 *Earth Surface Processes and Landforms*, 40, 1989-1999, [10.1002/esp.3601](https://doi.org/10.1002/esp.3601), 2015.

940 Vörösmarty, C. J., McIntyre, P. B., Gessner, M. O., Dudgeon, D., Prusevich, A., Green, P., Glidden, S.,  
941 Bunn, S. E., Sullivan, C. A., Liermann, C. R., and Davies, P. M.: Global threats to human water security  
942 and river biodiversity, *Nature*, 467, 555, [10.1038/nature09440](https://doi.org/10.1038/nature09440)  
943 <https://www.nature.com/articles/nature09440#supplementary-information>, 2010.

944 Wang, Q. J., and Robertson, D. E.: Multisite probabilistic forecasting of seasonal flows for streams with  
945 zero value occurrences, *Water Resources Research*, 47, [10.1029/2010wr009333](https://doi.org/10.1029/2010wr009333), 2011.

946 Wang, Q. J., Shrestha, D. L., Robertson, D. E., and Pokhrel, P.: A log-sinh transformation for data  
947 normalization and variance stabilization, *Water Resources Research*, 48, [doi:10.1029/2011WR010973](https://doi.org/10.1029/2011WR010973),  
948 2012.

949 Webb, J. A., and King, L. E.: A Bayesian hierarchical trend analysis finds strong evidence for large-scale  
950 temporal declines in stream ecological condition around Melbourne, Australia, *Ecography*, 32, 215-225,  
951 [doi:10.1111/j.1600-0587.2008.05686.x](https://doi.org/10.1111/j.1600-0587.2008.05686.x), 2009.

952 Whitworth, K. L., Baldwin, D. S., and Kerr, J. L.: Drought, floods and water quality: Drivers of a severe  
953 hypoxic blackwater event in a major river system (the southern Murray–Darling Basin, Australia),  
954 *Journal of Hydrology*, 450-451, 190-198, <https://doi.org/10.1016/j.jhydrol.2012.04.057>, 2012.

955 Zhang, Q., and Ball, W. P.: Improving riverine constituent concentration and flux estimation by  
956 accounting for antecedent discharge conditions, *Journal of Hydrology*, 547, 387-402,  
957 <https://doi.org/10.1016/j.jhydrol.2016.12.052>, 2017.

958 Zhang, Q.: Synthesis of nutrient and sediment export patterns in the Chesapeake Bay watershed:  
959 Complex and non-stationary concentration-discharge relationships, *Science of The Total Environment*,  
960 618, 1268-1283, <https://doi.org/10.1016/j.scitotenv.2017.09.221>, 2018.

961 Zhao, T., Schepen, A., and Wang, Q. J.: Ensemble forecasting of sub-seasonal to seasonal streamflow  
962 by a Bayesian joint probability modelling approach, *Journal of Hydrology*, 541, 839-849,  
963 <https://doi.org/10.1016/j.jhydrol.2016.07.040>, 2016.

964 Zhou, T., Wu, J., and Peng, S.: Assessing the effects of landscape pattern on river water quality at  
965 multiple scales: A case study of the Dongjiang River watershed, China, *Ecological Indicators*, 23, 166-  
966 175, <https://doi.org/10.1016/j.ecolind.2012.03.013>, 2012.

967

968

970 **Table 1. Key factors affecting the spatial and temporal variability for each of six constituents, as identified**  
 971 **in Lintern et al. (2018) and Guo et al. (2019b), respectively.**

Constituent	Key factors that affect spatial variability	Key factors that affect
<b>TSS</b>	Hottest month maximum temperature	Same-day streamflow
	Percentage area covered by grass	7-day antecedent streamflow
	Percentage area covered by shrub	Water temperature
	Percentage cropping area	Soil moisture root
	Maximum elevation	Soil moisture deep
	Dam storage	
	Percentage clay area	
<b>TP</b>	Erosivity	Same-day streamflow
	Percentage area covered by grass	30-day antecedent streamflow
	Percentage area covered by shrub	Water temperature
	Percentage area made up of roads	Soil moisture root
	Percentage cropping area	Soil moisture deep
	Average soil TP content	
<b>FRP</b>	Percentage area covered by shrub	Same-day streamflow
	Percentage cropping area	Water temperature
	Catchment area	Soil moisture deep
	Average soil TP content	
<b>TKN</b>	Mean channel slope	
	Percentage clay area	Same-day streamflow
	Warmest quarter mean temperature	30-day antecedent streamflow
	Coldest quarter rainfall	NDVI
	Percentage cropping area	Water temperature
	Percentage pasture area	Soil moisture root
<b>NO<sub>x</sub></b>	Average soil TP content	Soil moisture deep
	Annual radiation	Same-day streamflow
	Warm quarter rainfall	30-day antecedent streamflow
	Hottest month maximum temperature	NDVI
	Average soil TP content	Water temperature
	Mean channel slope	Soil moisture root
<b>EC</b>		Soil moisture deep
	Annual radiation	Same-day streamflow
	Annual rainfall	14-day antecedent streamflow
	Wettest quarter rain	Water temperature
	Hottest month maximum temperature	Soil moisture root
	Percentage agriculture area	Soil moisture deep
	Percentage cropping area	
Percentage area covered by shrub		
	Average soil TN content	

972

973 **Table 2. The key catchment landscape characteristics that are related to the varying relationships of water**  
 974 **quality and same-day streamflow across space, which were selected as the two predictors for the**  
 975 **streamflow effect in our model. Two characteristics were selected to summary the variability of**  
 976 **streamflow effects across space for each constituent, see Section 2.3 for details of the selection method. The**  
 977 **corresponding Spearman’s correlation (R, at p<0.05) between the effect of streamflow and each**  
 978 **catchment characteristic is presented.**

Constituent	Key factors that affect spatial variability in temporal effects	Spearman’s $\rho$ (p<0.05)
<b>TSS</b>	Annual rainfall	0.722
	Hottest month maximum temperature	-0.575
<b>TP</b>	Annual rainfall	0.695
	Percentage area used for cropping	-0.556
<b>FRP</b>	Percentage agriculture area	0.392
	Percentage area underlain by mixed igneous bedrock	0.314
<b>TKN</b>	Annual rainfall	0.713
	Hottest month maximum temperature	-0.618
<b>NO<sub>x</sub></b>	Total storage capacity of dams in catchment	-0.493
	Mean soil TN content	0.458
<b>EC</b>	Percentage area covered by grassland	-0.347
	Percentage area covered by woodland	-0.317

979

980 **Table 3. Comparison of model performance for all records and only the above-DL records for**  
 981 **each constituent.**

Constituent	Above-DL records only	All records
TSS	0.225	0.397
TP	0.433	0.445
FRP	-1.920	0.199
TKN	0.658	0.630
NO <sub>x</sub>	0.216	0.382
EC	0.907	0.886

982  
983

984 **Table 4. Model ability to capture observed water quality trends across all monitoring sites for**  
 985 **each constituent. The percentages of sites where observed positive and negative trends are**  
 986 **captured by the model are presented separately. Values in brackets indicate numbers of sites**  
 987 **where corresponding positive or negative trends are observed. For detailed estimation of these**  
 988 **percentages please refer to Sect. 2.2.**

Constituent	% positive trends captured	% negative trends captured
TSS	33.3 (12)	85.0 (20)
TP	82.1 (28)	16.7 (12)
FRP	47.1 (17)	55.6 (9)
TKN	81.1 (37)	40.0 (10)
NO <sub>x</sub>	68.6 (35)	66.7 (27)
EC	82.6 (23)	77.3 (22)

989

990 **Table 5. Comparison of model performances (as NSE) of the full model (Column 2) and the 50**  
 991 **partial models (Columns 3 to 5) with each calibrated to 80% randomly selected monitoring sites.**  
 992 **Columns 3 to 5 summarize the mean, minimum and maximum NSE values across the 50 runs,**  
 993 **where for each constituent, the top row showing calibration performance and the bottom row**  
 994 **showing the validation performance (i.e. at the 20% sites that were not used for calibration).**

Constituent	Full model	50 CV mean	50 CV min	50 CV max
TSS	0.397	0.413	0.376	0.439
		0.382	0.292	0.513
TP	0.445	0.461	0.427	0.501
		0.411	0.151	0.575
FRP	0.199	0.168	0.067	0.232
		0.129	-0.078	0.272
TKN	0.630	0.654	0.622	0.670
		0.622	0.468	0.691
NO <sub>x</sub>	0.382	0.453	0.414	0.489
		0.397	0.258	0.563
EC	0.886	0.893	0.882	0.903
		0.875	0.809	0.924

995

996 **Table 6. Comparison of model performances (as NSE) of the full model and the three models**  
 997 **that were calibrated to the pre-drought (1994-1996), drought (1997-2009) and the post-drought**  
 998 **(2010-2014) periods. For each of the models, the calibration performance is shown on the top**  
 999 **row and the validation performance (i.e. over the periods that were not used for calibration) is**  
 1000 **shown on the bottom row.**

Constituent	Full model	Pre-drought calibration	During drought calibration	Post-drought calibration
TSS	0.397	0.495	0.399	0.499
		0.208	0.402	0.390

TP	0.445	0.477	0.438	0.525
		0.421	0.474	0.411
FRP	0.199	-1.336	0.187	0.204
		-1.406	0.197	0.024
TKN	0.630	0.649	0.650	0.711
		0.566	0.648	0.610
NOx	0.382	0.443	0.426	0.509
		0.394	0.471	0.393
EC	0.886	0.854	0.901	0.901
		0.887	0.873	0.884

1001